

Exponential Quantum Speedup for Simulation-Based Optimization Applications

Jonas Stein,^{1,2,*} Lukas Müller,³ Leonhard Hölscher,³ Georgios Chnitudis,³ Jezer Jojo,⁴ Afrah Farea,⁵ Mustafa Serdar Çelebi,⁵ David Bucher,² Jonathan Wulf,¹ David Fischer,¹ Philipp Altmann,¹ Claudia Linnhoff-Popien,¹ and Sebastian Feld⁶

¹*Institute for Informatics, LMU Munich*

²*Aqarios GmbH, Munich*

³*BMW Group, Munich*

⁴*Indian Institute of Science Education and Research Pune*

⁵*Istanbul Technical University*

⁶*Quantum & Computer Engineering, Delft University of Technology*

(Dated: September 17, 2024)

The simulation of many industrially relevant physical processes can be executed up to exponentially faster using quantum algorithms. However, this speedup can only be leveraged if the data input and output of the simulation can be implemented efficiently. While we show that recent advancements for optimal state preparation can effectively solve the problem of data input at a moderate cost of ancillary qubits in many cases, the output problem can provably not be solved efficiently in general. By acknowledging that many simulation problems arise only as a subproblem of a larger optimization problem in many practical applications however, we identify and define a class of practically relevant problems that does not suffer from the output problem: Quantum Simulation-based Optimization (QuSO). QuSO represents optimization problems whose objective function and/or constraints depend on summary statistic information on the result of a simulation, i.e., information that can be efficiently extracted from a quantum state vector. In this article, we focus on the LinQuSO subclass of QuSO, which is characterized by the linearity of the simulation problem, i.e., the simulation problem can be formulated as a system of linear equations. By cleverly combining the quantum singular value transformation (QSVT) with the quantum approximate optimization algorithm (QAOA), we prove that a large subgroup of LinQuSO problems can be solved with up to exponential quantum speedups with regards to their simulation component. Finally, we present two practically relevant use cases that fall within this subgroup of QuSO problems.

I. INTRODUCTION

Initially motivated by Richard Feynman [1], one of the main quantum applications with provable exponential speedups is the simulation of physical and chemical systems. While this idea was historically targeted at the simulation of quantum mechanical systems [2], the discovery of a quantum algorithm for solving systems of linear equations, that also provides an exponential speedup in terms of the number of unknowns [3–10], extended this notion to the simulation of many classical physical systems. Since then, significant quantum speedups have been proven for many (potentially) practically relevant problems [11–14], based on techniques to formulate differential equations into an efficiently solvable format for quantum algorithms [15, 16]. Through linearization [17–19] or linear representations [20–22], even many non-linear differential equations have been shown to allow for exponential quantum speedups.

In the simulation of linear classical physical systems the biggest concern has historically been the data input to and the output from the quantum algorithm (cf., e.g., Ref. [3]).

Concerning the input problem, most literature either assumes the existence of quantum oracles providing ac-

cess to the inputs or even QRAM [23] (for which efficient hardware realization has shown to be very difficult). While the input of specific, mathematically highly structured matrices is starting to be explored (cf. [24, 25]), generally applicable approaches have not yet been established. As our first key contribution of this article, we show how recent results on provably optimal quantum state preparation [26, 27] can be used to efficiently prepare sparse matrices by combining them with the encoding approach from Ref. [7].

Addressing the output problem, it is important to acknowledge that any form of quantum state tomography necessary to extract all amplitudes of a given n -qubit quantum state vector takes $\mathcal{O}(2^n)$ many steps [28], which destroys any exponential quantum speedup achieved during the computation of this state. However, it is possible to efficiently extract some information from a quantum state using quantum algorithms like quantum phase estimation or the Hadamard test. As our second core contribution, we compile a comprehensive framework of quantum algorithms that can efficiently extract information (often called summary statistic information, cf. [3]) from a state vector.

By acknowledging that real world academic and industrial simulation problems often occur in context of a larger optimization problem, one can recognize that the relevant information about the result of the simulation problem can in fact be efficiently extracted by a quan-

* jonas.stein@ifi.lmu.de

tum algorithm for many practically relevant use cases. Concrete examples entail so-called simulation-based optimization problems, i.e., problems about finding input parameters to a simulation model that optimize a given objective¹ [33], which can be found in many areas of application and research such as pharmaceutical development [34] or aircraft design [35]. We later formalize the class of simulation-based optimization problems that do not suffer from the output problem via a corresponding definition of Quantum Simulation-based Optimization (QuSO). The central problem inherent to simulation-based optimization is that the computation of the objective value for every probed solution is very costly, such that often, only a very small subset of possible solutions can be explored (see e.g. Refs. [33, 36, 37]).

As our main contribution in this article, we show that exactly this connection of simulation and optimization components makes simulation-based optimization problems extremely well suited to quantum computing. We show that by cleverly combining the state-of-the-art quantum algorithms for optimization (QAOA) and solving systems of linear equations (QSVT), the output problem can be bypassed and the search space can be efficiently explored. Further, we provide an extensive complexity analysis and exemplify its practical application for two industrially relevant use cases: The unit commitment problem focused on optimal power flow and a basic form of topology optimization.

Notation: For arbitrary $n \in \mathbb{N}$, we use the notation $[n] := \{1, \dots, n\}$. We write \mathbb{I} for an identity matrix of size that is clear by the context. In quantum circuits, we denote a (multi-)controlled Z -gate with connected \bullet symbols (unless they are connected to any other gates, then this symbol denotes the usual control-operator). This is well-defined, as the position of the Z -gate in a (multi-)controlled Z -gate does not change the operator. If the controlled gate should actuate on the $|0\rangle$ state, the \circ symbol is used instead. We use $\|\cdot\|_2$ to denote the spectral norm, i.e., the largest singular value of the given matrix.

II. PRELIMINARIES

This section provides a formal definition of QuSO, basics on quantum optimization with the QAOA and established (partly reformulated) quantum algorithms for data input, data processing, and data output relevant for solving QuSO problems.

A. Quantum Simulation-based Optimization

In the following, we define the set of QuSO problems as a subset of MINLP, the most general group of practically relevant optimization problems. Note that we only consider minimization problems wlog.

Definition 1 (MINLP). *A Mixed-Integer Nonlinear Programming (MINLP) problem is an optimization problem of the form*

$$\begin{aligned} & \underset{x}{\text{minimize}} && f(x) \\ & \text{subject to} && c_j(x) \leq 0, \forall j \in [K], \\ & && x_i \in [l_i, u_i] \subset \mathbb{R}, \\ & && x_i \in \mathbb{Z}, \forall i \in I \subseteq [N], \end{aligned}$$

where $f : \mathbb{R}^N \rightarrow \mathbb{R}$ and $c : \mathbb{R}^N \rightarrow \mathbb{R}^K$ are continuous functions.

As we define QuSO based on the concept of summary statistic information, we now formally state what is generally understood under this term.

Definition 2 (Summary Statistic Information). *Given an oracle O that prepares an n -qubit quantum state $|\psi\rangle = O|0\rangle^{\otimes n}$, we define summary statistic information about $|\psi\rangle$ as the output of a quantum algorithm that yields a basis-encoded binary string that depends on $|\psi\rangle$ given access to O .*

Definition 3 (Quantum simulation-based optimization). *We define a quantum simulation-based optimization (QuSO) problem as a MINLP problem whose objective function and/or constraints depend on the summary statistic result of a simulation problem, i.e.,*

$$\begin{aligned} & \underset{x}{\text{minimize}} && f(x, u(s(x))) \\ & \text{subject to} && c_j(x, u(s(x))) \leq 0, \forall j \in [K], \\ & && x_i \in [l_i, u_i] \subset \mathbb{R}, \\ & && x_i \in \mathbb{Z}, \forall i \in I \subseteq [N], \end{aligned}$$

where $f : \mathbb{R}^N \times \{0, 1\}^m \rightarrow \mathbb{R}$ and $c : \mathbb{R}^N \times \{0, 1\}^m \rightarrow \mathbb{R}^K$ are continuous functions, and $s : \mathbb{R}^N \rightarrow \mathbb{R}^M$ represents a simulation problem of which summary statistic information can be efficiently extracted via the function $u : \mathbb{R}^M \rightarrow \{0, 1\}^m$.

This class of optimization problems is designed to entail all simulation-based optimization problems that could potentially allow for a quantum speedup for their simulation components. Apart from our area of focus in this paper—linear simulation problems—QuSO also contains important problems involving non-linear simulations, e.g., based on the Navier-Stokes equations [38]. Note that QuSO does not differentiate between “quantum problems“, like finding the ground state of an electronic structure, or “classical problems“ like the simulation of structural mechanics, QuSO merely specifies

¹ Note that a large body of research in simulation-based optimization investigates simulations of stochastic functions, which we do not – we exclusively consider deterministic simulations. More precisely, we only consider parametric (i.e., static) optimization, i.e., we only consider the system of interest’s properties in one specific real world configuration (cf. [29–32]).

that the information about the result of the simulation problem required by the optimization problem can be extracted efficiently. In this context, *efficiently* means that the computational complexity of extracting the summary statistic information does not outweigh a potential quantum speedup gained through a faster simulation.

Definition 4 (Linear Quantum simulation-based optimization). *We define a linear quantum simulation-based optimization (LinQuSO) problem as a QuSO problem for which the underlying simulation problem takes the form of a system of linear equations (SLE) for all possible solutions.*

In this paper, we provide a framework to construct a quantum algorithm to solve LinQuSO problems of many common forms, allowing for an exponential speedup of the simulation component if all of the following conditions are satisfied.

1. The SLE is sparse and well-conditioned.
2. The dependence of the SLE on the decision variables allows for an efficient input to a quantum linear system solver. (For details see Sec. III A)
3. The extraction of summary statistic information from the result of the SLE can be done as efficiently as the simulation. (For details see Sec. III C)

B. Quantum Optimization

As an approximated form of the Quantum Adiabatic Algorithm (QAA) [39], the QAOA utilizes the Adiabatic Theorem [40] to approximate the solutions of unconstrained² combinatorial optimization problems [43]. Given a binary³ objective function $f : \{0, 1\}^n \rightarrow \mathbb{R}$, this is accomplished by:

1. Mapping the objective values onto the energy levels of a Hamiltonian $H_C = \sum_x f(x) |x\rangle\langle x|$.
2. Preparing a system in the ground state of a Hamiltonian, i.e., usually $|+\rangle^{\otimes n}$ for $H_M = -\sum_{i=1}^n \sigma_i^x$.
3. Simulating the time evolution $\exp(i \int_0^T H_s(t) dt)$ approximatively, where $H_s(t) = (1 - s(t)) H_M + s(t) H_C$ governs the adiabatic evolution and $s : [0, T] \rightarrow [0, 1]$ monotonically transitions from 0 to 1 for any given time $T > 0$.
4. Measuring the resulting state $|\psi\rangle$ and remapping it to its corresponding solution of the objective function f .

To simulate the time evolution governed by H_s on gate-based quantum computers, a discretization into $p \in \mathbb{N}$ Hamiltonians $H_s(1/T), \dots, H_s(T)$, as well as first order Suzuki-Trotter approximation is applied to yield the following unitary time evolution describing the QAOA:

$$U(\beta, \gamma) = U_M(\beta_p) U_C(\gamma_p) \dots U_M(\beta_1) U_C(\gamma_1), \quad (1)$$

where β_i and γ_i characterize the speed of the time evolution and $U_M(\beta_i) = e^{-i\beta_i H_M}$, $U_C(\gamma_i) = e^{-i\gamma_i H_C}$, such that $U(\beta, \gamma)$ approaches adiabatic evolution for $p \rightarrow \infty$, and constant speed, i.e., $\beta_i = 1 - i/p$, and $\gamma_i = i/p$ [45]. This is formally stated in Thm. 1.

Theorem 1 (Quantum Approximate Optimization Algorithm [43, 45]). *Given an objective function $f : \{0, 1\}^n \rightarrow \mathbb{R}$, the quantum circuit defined by $U(\beta, \gamma)$ in Eq. (2) yields $\arg \min_x f(x)$ for $p \rightarrow \infty$, and $\beta_i := 1 - i/p$, and $\gamma_i := i/p$.*

$$U(\beta, \gamma) := U_M(\beta_p) U_C(\gamma_p) \dots U_M(\beta_1) U_C(\gamma_1) H^{\otimes n}, \quad (2)$$

where $U_M(\beta_i) := e^{-i\beta_i H_M}$, $U_C(\gamma_i) := e^{-i\gamma_i H_C}$, $H_C := \sum_x f(x) |x\rangle\langle x|$, and $H_M := -\sum_{i=1}^n \sigma_i^x$.

The key difference between pure adiabatic time evolution (as in the QAA) and the QAOA is the introduction of the parameters β and γ , which allow for non-linear evolution speed. This is a crucial benefit, as the maximal evolution speed allowed by the adiabatic theorem at any given point in time t depends on the spectral gap (i.e., the energy gap between the ground state and the first excited state of the continuous-time Hamiltonian $H(t)$), which is computationally intractable in the general case [43]. Through the parameterization of this time evolution speed, machine learning techniques can be used to optimize it [46], which can significantly increase the solution quality under restricted runtime [43].

Note that as proposed in Ref. [47], the QAOA can be adapted to handle constraints in form of a reduced space of feasible solutions $F \subseteq \{0, 1\}^n$ given by a state preparation operator $U_s : |0\rangle^{\otimes n} \mapsto |F\rangle$, where $|F\rangle$ a superposition of all feasible solutions.

Lemma 1 (Grover Mixer [47]). *By adapting $U_M(\beta_i) := e^{-i\beta_i |F\rangle\langle F|}$ and $U(\beta, \gamma)$ as in Eq. (3),*

$$U(\beta, \gamma) := U_M(\beta_p) U_C(\gamma_p) \dots U_M(\beta_1) U_C(\gamma_1) U_s, \quad (3)$$

the space of explored solutions in the QAOA can be limited to $F \subseteq \{0, 1\}^n$. When $|F\rangle$ is an equal superposition over all states in F , solutions with the same solution quality are sampled with equal probability.

C. Data input

Efficient data input to quantum algorithms has been an intensive area of research in recent years. The key insight that emerged during this process is an efficient

² To incorporate constraints, the standard approach penalty terms can be introduced (see, e.g., Ref. [41]), or more sophisticated approaches (see, e.g., Ref. [42]) can be used.

³ For any non-binary domains, a suitable encoding onto $\{0, 1\}^n$ must be conducted (see, e.g., Ref. [44]).

implementation of a uniformly controlled gate using arbitrary amounts of ancillary qubits [26]. This result allows for solving the well-known input problem in quantum computing by trading off runtime with space, i.e., the quantum statevector $|\psi\rangle$ of an arbitrary normalized vector $\psi \in \mathbb{R}^N$ can be prepared in time $\mathcal{O}(\log_2 N)$ if $\mathcal{O}(N)$ ancilla qubits are available, where $n \in \mathbb{N}$ s.t. $N = 2^n$. As we will make use of this idea at many points in the paper, we now introduce these concepts more formally.

Definition 5 (Uniformly Controlled Unitary [27]). *Given a collection of 2^k many l -qubit unitary matrices $U_0, U_1, \dots, U_{2^k-1}$, we call the block-diagonal matrix $\text{diag}(U_0, \dots, U_{2^k-1})$ a (k, l) -uniformly controlled unitary (UCU). If $l = 1$, we use the term uniformly controlled gate (UCG) instead. A quantum circuit implementation of a (k, l) -UCU is displayed in Fig. 1.*

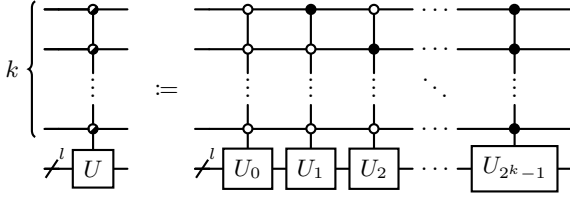


FIG. 1. Quantum circuit implementation of a (k, l) -UCU as defined in Def. 5. The \bullet symbol is used as shorthand to iterate over all possible control combinations on the applied wire.

Lemma 2 (Implementing UCGs [26, Lem. 12]). *Any n -qubit UCG can be implemented by a quantum circuit of depth $\mathcal{O}(n + 2^n/n+m)$ using $m \in \mathbb{N}_0$ ancillary qubits.*

Lemma 3 (Quantum State Preparation [26, Thm. 1]). *Any n -qubit quantum state $|\psi\rangle$ can be prepared by a quantum circuit of depth $\mathcal{O}(n)$ using $\mathcal{O}(2^n)$ ancillary qubits.*

Theorem 2 (Controlled Quantum State Preparation [27, Thm. 1]). *For any set of n -qubit quantum states $\{|\psi_i\rangle : i \in \{0, 1\}^k\}$, a depth $\mathcal{O}(n + k + 2^{n+k}/n+k+m)$ quantum circuit performing the controlled state preparation $|i\rangle|0\rangle^{\otimes n} \mapsto |i\rangle|\psi_i\rangle \forall i$ (i.e., a uniformly controlled unitary) can be implemented using $m \in \mathbb{N}_0$ ancillary qubits.*

Remark 1. Let $2^k = K \in \mathbb{N}$ and $2^n = N \in \mathbb{N}$. When given access to $N \cdot K$ ancillary qubits, the algorithm provided by Thm. 2 enables the state preparation of K normalized N -dimensional vectors $b_x \in \mathbb{R}^N \forall x \in \{0, 1\}^k$ in a quantum circuit of depth $\mathcal{O}(\log_2(K) + \log_2(N))$.

Lemma 4 (Polynomial Quantum Arithmetic [48, Appendix B]). *Given an n -qubit state $|x\rangle$ of a basis encoded binary number $x \in [-1, 1]$, we can implement a unitary operator $|x\rangle \mapsto |f(x)\rangle$ in a quantum circuit of depth $\mathcal{O}(n^2d)$ using $\mathcal{O}(nd)$ ancillas for any bijective d -degree polynomial $f \in \mathbb{R}[x]$ with $|f(x)| \leq 1 \forall x$.*

Lemma 5 (Ancilla Quantum Encoding). *Given a basis encoded quantum state $|x\rangle := |x_1 \dots x_n\rangle$ in two's complement (i.e., the binary string $x_1 \dots x_n$ represents the number $x = -\frac{1}{2}x_1 + \sum_{i=2}^n x_i 2^{-i} \in [-0.5, 0.5[$), we can implement ancilla quantum encoding (AQE), i.e., the unitary operator mapping x onto an amplitude as in $|0\rangle|x\rangle \mapsto x|0\rangle|x\rangle + \sqrt{1-x^2}|1\rangle|x\rangle$, with a quantum circuit of depth $\mathcal{O}(n)$ and $\mathcal{O}(2^n)$ ancillary qubits or depth $\mathcal{O}(n^2/\varepsilon)$ and $\mathcal{O}(n/\varepsilon)$ ancillas, where ε denotes the error.*

Proof. For the error dependent case see [49] and [48, Appendix B]. The error-free case is based on a lookup table approach (cf. [49]) where each possible x is processed using a respectively controlled R_y rotation with classically precomputed rotation angles. This approach takes the form of a uniformly controlled gate, which can be implemented in the stated depth using $\mathcal{O}(2^n)$ ancillas based on Lem. 2. \square

When solving an $A\vec{x} = \vec{b}$ type SLE on a quantum computer, one identifies the (necessarily normalized and potentially 0-padded) vector \vec{b} with a statevector $|b\rangle$, and the (necessarily $\|\cdot\|_2$ -normalized) matrix A with a unitary operator U_A that block-encodes A , i.e.,

$$U_A = \begin{pmatrix} A & * \\ * & * \end{pmatrix}. \quad (4)$$

For any SLE that does not already take this form, the result of any quantum linear system solver for x takes the (potentially 0-padded) form $|x\rangle = A^+ \vec{b} / \|A^+ \vec{b}\|_2$. To simplify notation (and to avoid clutter), we assume sufficient normalization (and padding) for A , \vec{b} and \vec{x} respectively in the following if not indicated otherwise.

In the following we formally define the notion of block-encoding, and provide a concrete quantum circuit implementation to synthesise the corresponding unitary operator. Note that block-encoding implementations frequently entail a so called subnormalization factor, i.e., they block-encode A/α with $\alpha > 1$ instead of A . As the circuit depth of state-of-the-art quantum linear system solvers typically depends linearly on α we focus on an implementation of block-encoding that minimizes subnormalization (cf. Lem. 6).

Definition 6 (Block-encoding). *For any matrix $A \in \mathbb{C}^{2^l \times 2^r}$, an $(n+a)$ -qubit unitary U_A is an (α, a, ε) -block-encoding of A , if*

$$\left\| A - \alpha \left(\langle 0 |^{\otimes a} \otimes I^{\otimes l} \right) U \left(|0\rangle^{\otimes a} \otimes I^{\otimes r} \right) \right\| \leq \varepsilon. \quad (5)$$

Lemma 6 (Block-encoding sparse-access matrices [7, Lem. 48]). *Assume sparse-access to an s_r -row- and s_c -column-sparse matrix $A \in \mathbb{R}^{2^n \times 2^n}$ with $|a_{ij}| \leq 1$, i.e., we have access to the oracles*

$$\begin{aligned} O_r &: |i\rangle|k\rangle \mapsto |i\rangle|r_{ik}\rangle & \forall i \in [2^n - 1], k \in [s_r] \\ O_c &: |l\rangle|j\rangle \mapsto |c_{lj}\rangle|j\rangle & \forall l \in [s_c], j \in [2^n - 1] \\ O_A &: |i\rangle|j\rangle|0\rangle^{\otimes e} \mapsto |i\rangle|j\rangle|\tilde{a}_{ij}\rangle & \forall i, j \in [2^n - 1] \end{aligned}$$

where r_{ik} is the index of the k -th non-zero entry of the i -th row of A and $k+2^n$ if there are less than i non-zero entries, c_{lj} is defined analogously, and \tilde{a}_{ij} is a $\lceil \log_2 1/\varepsilon_1 \rceil$ -bit binary approximation of a_{ij} s.t. $|a_{ij} - \tilde{a}_{ij}| \leq \varepsilon_1$. Then we can implement a $(\sqrt{s_r s_c}, n+3, \varepsilon_1 + \varepsilon_2)$ -block-encoding of A using the quantum circuit described in Fig. 2, which requires a single use of O_R and O_C , two uses of O_A , $\mathcal{O}(n + \log^{2.5}(s_r s_c / \varepsilon_2))$ one and two qubit gates and $\mathcal{O}(\log 1/\varepsilon_1, \log^{2.5}(s_r s_c / \varepsilon_2))$ ancillas. Here, ε_2 denotes the error resulting from an AQE of the values of the matrix entries.

Proof. The only difference to the original formulation of this lemma in Ref. [7] is the added error-tolerance for the entries ε_1 , which contributes practically linearly to the total error as the only function applied to the matrix entries (i.e., arccos during AQE) is basically linear near 0. Thus the stated error dependence is slightly approximative, but accurate enough for our means, especially when assuming ε_1 to be small. \square

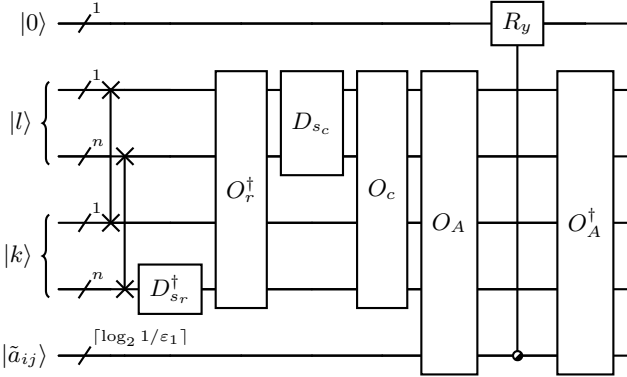


FIG. 2. Circuit of a $(\sqrt{s_r s_c}, n+3, \varepsilon_1 + \varepsilon_2)$ -block-encoding of a matrix A given corresponding sparse-access oracles O_r , O_c , and O_A as defined in Lem. 6. D_s is defined as the map $|0\rangle^{\otimes q} \mapsto \frac{1}{\sqrt{s}} \sum_{k=1}^s |k\rangle$ (with $2 \leq s \leq 2^q$ – for an implementation requiring no ancillary qubits and a depth of $\mathcal{O}(\log_2 s)$ see Ref. [50]). Purely for notational simplicity, AQE is visualized by a uniformly controlled R_y rotation (cf. Lem. 5).

Remark 2. In the case of $\|A\|_2 \leq 1/2$, the subnormalization factor can be amplified to $\sqrt{2n_r n_c}$ (where $n_r \in [1, s_r]$ is an upper bound on $\|a_{i\cdot}\|_q^q$ and $n_c \in [1, s_c]$ is an upper bound on $\|a_{\cdot j}\|_{2-q}^{2-q}$ with $q \in [0, 2]$) using uniform spectral gap amplification (for details, see [7, Lem. 49]), which we omit for ease of readability.

Corollary 1. As a consequence of Lem. 6, the speedup that we can gain (assuming a sufficiently well-conditioned SLE) from a quantum algorithm using this kind of block encoding depends on the sparsity. While an exponential speedup is possible for matrices whose sparsity is maximally logarithmic wrt. the systems dimensions, the worst case runtime for dense matrices scales with $\mathcal{O}(N)$.

Proof. Acknowledge $s_r, s_c \leq N$ in Lem. 6, thus the subnormalization factor is upper bound by N . \square

Note that this leads to a worst case quantum speedup of $\mathcal{O}(N^2)$ compared to the best classical approach (the Conjugate-Gradient method, which has complexity $\mathcal{O}(Ns\kappa \log(1/\varepsilon))$) when assuming a sufficiently well-conditioned SLE. If the condition number scales badly, we have to compare against the classical Gaussian elimination approach, which takes $\mathcal{O}(N^3)$ time.

Remark 3. Given QRAM access to the matrix A (for a definition of QRAM, see [51])⁴, the circuit depth for a quantum linear systems solver for dense SLEs can be reduced to $\mathcal{O}(\kappa^2 \sqrt{N} \text{polylog}(N)/\varepsilon)$ [52]. However, this approach is based on an entirely different algorithm (the Quantum Singular Value Estimation [23]), which works based on quantum phase estimation and hence has an exponentially worse dependence on the error compared to QSVT. Note that this runtime can be improved to $\mathcal{O}(\kappa^2 \sqrt{N} \text{polylog}(\kappa/\varepsilon))$ if we also have access to an Linear Combination of Unitaries (LCU) decomposition of our matrix (which is generally not the case for practically relevant problems), by using the approach described in [53].

D. Quantum Linear Algebra Subroutines

In this section, we show how Quantum Singular Value Transformation can be used to solve SLEs. Historically, QSVT is a generalization of Quantum Signal Processing (QSP). QSP is motivated from Ref. [54] and was later formally proposed in Ref. [55].

Theorem 3 (Quantum Signal Processing [7, Thm. 5]). *Given an operator $W(x) := R_x(-2 \arccos x)$ and a polynomial $P \in \mathbb{C}[x]$, we can find phase angles $\phi_1, \dots, \phi_{d+1} \in \mathbb{R}$ and a polynomial $Q \in \mathbb{C}[x]$ such that*

$$e^{i\phi_1 \sigma_z} \prod_{k=1}^{d+1} W(x) e^{i\phi_k \sigma_z} = \begin{bmatrix} P(x) & iQ(x)\sqrt{1-x^2} \\ iQ^*(x)\sqrt{1-x^2} & P^*(x) \end{bmatrix}$$

when $\tilde{P} := \text{Re}(P)$ satisfies (i) $\deg(\tilde{P}) \leq d$, (ii) \tilde{P} has parity $d \bmod 2$, and (iii) $\tilde{P}(x)^2 \leq 1$, for all $x \in [-1, 1]$.

Proof. Special case ($\text{Re}(Q) \equiv 0$) of Thm. 5 in Ref. [7]. \square

Remark 4. Usually, one is only interested in the real part of P in Thm. 3. To acquire a unitary operation that performs $\text{Re}(P(x))$ rather than $P(x)$, we can use that $\text{Re}(P(x)) = \frac{1}{2}(P(x) + P^*(x))$ in combination with the approach elaborated in Lem. 52 of Ref. [7] to implement

⁴ While no hardware implementing QRAM is available at the time this article is published, one could use CQSP (cf. Thm. 2) as a quantum circuit implementation of it at the cost of quadratically many ancillas wrt. the SLE's dimension.

such linear combination of unitary matrices as a $(1, 1 + 1, 0)$ -block-encoding

$$\begin{bmatrix} \text{Re}(P(x)) & * \\ * & * \end{bmatrix} |0\rangle |\psi\rangle = \begin{array}{c} |0\rangle \\ |\psi\rangle \end{array} \begin{array}{c} \text{---} [H] \text{---} \\ \text{---} [U_\phi] \text{---} \\ \text{---} [U_\phi^\dagger] \text{---} \\ \text{---} [H] \text{---} \end{array}$$

where U_ϕ denotes the unitary operator proposed in Thm. 3, i.e., $U_\phi := e^{i\phi_0\sigma_z} \prod_{k=1}^d W(x)e^{i\phi_k\sigma_z}$. Note that this circuit also works for block encodings of arbitrary complex matrices A instead of the scalar entry considered for U_ϕ .

Remark 5. The state-of-the-art phase angle calculation approach for QSP (i.e., Ref. [56]) is based on Newton's method and takes $\mathcal{O}(d^2)$ steps to converge in practice, which can pose severe limitations to highly ill-conditioned systems of equations. However, recently, a generalized form of QSP (GQSP) was proposed by Montlagh and Wiebe in Ref. [57] which allows for an $\mathcal{O}(d \log d)$ time algorithm to calculate the phase angles. The key to achieve this speedup is the generalization to arbitrary rotations in the signal processing operator by lifting the limitation of purely applying rotations in the z -axis. Based on this idea, Sünderhauf has proposed a corresponding generalization of the quantum singular value transformation algorithm (GQSVT), which uses the same quasi-linear approach to calculate the phase angles [58]. As the GQSVT has the same computational complexity as the QSVT apart from the faster phase angle calculation, we only discuss the more well-known QSVT in the following for the sake of brevity.

Theorem 4 (Quantum Singular Value Transformation [59, Thm. 4]). *Given a matrix $A \in \mathbb{C}^{L \times R}$ with singular value decomposition $\sum_k \sigma_k |w_k\rangle \langle v_k|$ through a corresponding (α, a, ε) -block-encoding U_A , we can implement an (α, a, ε) -block-encoding of $P(A) := \sum_k P(\sigma_k) |w_k\rangle \langle v_k|$ for any given odd polynomial $P \in \mathbb{C}[x]$ of degree d satisfying conditions (i) – (iii) from Thm. 3 via the unitary operator*

$$\tilde{\Pi}_{\phi_1} U_A \prod_{k=1}^{(d-1)/2} \left(\Pi_{\phi_{2k}} U_A^\dagger \tilde{\Pi}_{\phi_{2k+1}} U_A \right) \Pi_{\phi_{d+1}},$$

and respectively $P(A) := \sum_k P(\sigma_k) |v_k\rangle \langle v_k|$ for an even polynomial $P \in \mathbb{C}[x]$ of degree d via

$$\prod_{k=1}^{d/2} \left(\Pi_{\phi_{2k-1}} U_A^\dagger \tilde{\Pi}_{\phi_{2k}} U_A \right) \Pi_{\phi_{d+1}},$$

where $\tilde{\Pi}_{\phi_k} := e^{i\phi_k(2\tilde{\Pi}-\mathbb{I})}$ and $\Pi_{\phi_k} := e^{i\phi_k(2\Pi-\mathbb{I})}$ denote the so-called projector-controlled phase shift operators with phase angles ϕ_k analog to Thm. 3. These are based on the orthogonal projectors (i.e., idempotent Hermitians) $\tilde{\Pi} := |0\rangle^{\otimes m-l} \langle 0|^{\otimes m-l} \otimes I^{\otimes l}$ and $\Pi := |0\rangle^{\otimes m-r} \langle 0|^{\otimes m-r} \otimes I^{\otimes r}$ for $m := n + a$ that locate A in its given block-encoding.

Employing a single ancillary qubit for the implementation of the projector-controlled phase shift operators, we can implement the full QSVT procedure via the quantum circuits displayed in Fig. 3.

Remark 6. While the phase angles for QSP and QSVT are identical [7, Thm. 17], note that slightly altered versions of the proposed circuits exist in literature, which may demand a specific shift for each phase angle (for details, see Ref. [60]). For practical implementation, there is open source code available to calculate the phase angles. A state-of-the-art approach can be found in the Newton method from QSPACK – note though, that for the implementation to work with our definition of QSVT, one has to shift its first and last angle output by $-\pi/4$.

Theorem 5 (Quantum Moore-Penrose Pseudoinverse [7, Thm. 41]). *Given $A \in \mathbb{C}^{L \times R}$ with singular value decomposition $A = W\Sigma V^\dagger$, an upper bound σ_{\max}^* on its maximal singular value σ_{\max} and a lower bound $\sigma_{\min}^* > 0$ on its minimal non-zero singular value σ_{\min} , we can implement a $(2/\sigma_{\min}^*, a + 1, \varepsilon_2 + \varepsilon_1/2\sigma_{\max}^*(\sigma_{\min}^* - \varepsilon_1))$ -block-encoding of its pseudoinverse A^+ using QSVT on a $(\sigma_{\max}^*, a, \varepsilon_1)$ -block-encoding of A with an odd polynomial of degree $\mathcal{O}(\kappa^* \log(\kappa^*/\varepsilon_2))$ that approximates $\sigma_{\min}^*/2\sigma_{\max}^*x$, where $\kappa^* := \sigma_{\max}^*/\sigma_{\min}^*$, $A^+ := V\Sigma^{-1}W^\dagger$, and Σ^{-1} denotes the element-wise inverse of the non-zero elements of Σ . For the error in the resulting block-encoding, it is assumed that $\varepsilon_1 \ll \sigma_{\min}^*$, which is an obvious constraint if one cares about all small singular values being inverted with high accuracy.*

Proof. This is a result of Thm. 41 from Ref. [7] when plugging in an ε_1 -approximation of the (sub-)normalized version of A as specified. The additive dependence of the error term $\varepsilon_1/2\sigma_{\max}^*(\sigma_{\min}^* - \varepsilon_1)$ in the resulting block-encoding of A^+ can be computed straightforwardly with the stated assumption of $\varepsilon_1 \ll \sigma_{\min}^*$ by focusing on the smallest singular value. \square

Corollary 2 (Quantum Linear System Solving [61]). *Given a system of linear equations $A\vec{x} = \vec{b}$ with $A \in \mathbb{R}^{2^l \times 2^r}$, an upper bound σ_{\max}^* on its maximal singular value, a lower bound $\sigma_{\min}^* > 0$ on its minimal non-zero singular value as well as U_A , a $(\sigma_{\max}^*, a, \varepsilon_1)$ -block-encoding of A and an oracle preparing $U_b |0\rangle^{\otimes l} = |b\rangle := \vec{b}/\|\vec{b}\|_2$, we can implement a quantum circuit yielding an $(\varepsilon_2 + \varepsilon_1/2\sigma_{\max}^*(\sigma_{\min}^* - \varepsilon_1))$ -approximation of the quantum statevector $|x\rangle := A^+ \vec{b}/\|A^+ \vec{b}\|_2$ with a single initial query of U_b and $\mathcal{O}(\kappa^* \log(\kappa^*/\varepsilon_2))$ subsequent sequential queries to U_A using one ancillary qubit as described in Thm. 5. Note that for an extraction of $|x\rangle$, a $|0\rangle$ post-selection on the $a + 1$ ancillary qubits is necessary. This post-selection has success probability $(\sigma_{\min}^* \|A^+ |b\rangle\|_2 / 2)^2 \in [(1/2\kappa^*)^2, (1/2)^2]$ and can be amplified to a value $\geq 1/2$ using $\mathcal{O}(\kappa^*)$ rounds of amplitude amplification.*

Proof. The stated form of a quantum linear systems solver is a direct result of applying the Moore-Penrose

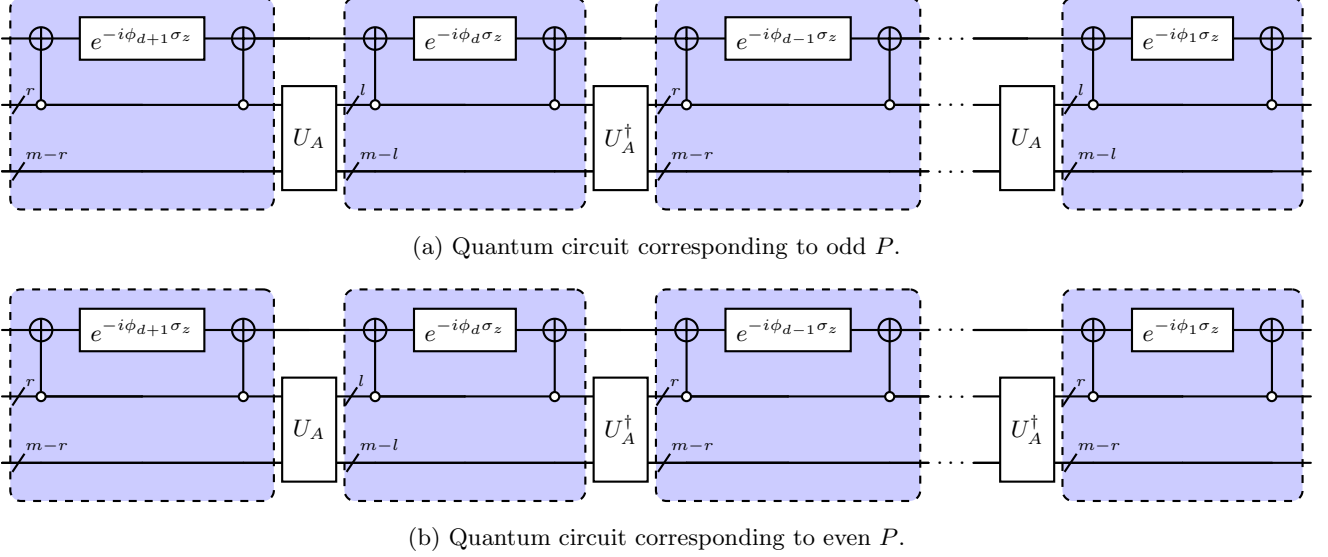


FIG. 3. Quantum circuits implementing an $(\alpha, a + 1, \varepsilon)$ -block-encoding of $P(A)$ via QSVT for arbitrary given $A \in \mathbb{C}^{L \times R}$ and even or odd polynomials $P \in \mathbb{C}[x]$. The blue boxes show implementations of projector-controlled phase shift operators $\tilde{\Pi}_{\phi_k}$ and Π_{ϕ_k} using a clean ancillary qubit from the top wire.

inverse from Thm. 5 onto $|b\rangle$. For details on the post-selection, see Ref. [61]. \square

Remark 7 (Rescaling $|x\rangle$). As described in Cor. 2, our quantum linear system solver yields the quantum state $|x\rangle = A^+ \vec{b} / \|A^+ \vec{b}\|_2$, which is merely a rescaled version of the actual result $\vec{x} = A^+ \vec{b}$. As a classical calculation of the factor $\|A^+ \vec{b}\|_2$ would generally require solving the SLE, any quantum speedup would be lost by the classical overhead to compute this scaling factor. Fortunately, we can use Quantum Amplitude Estimation (QAE) on the state of the ancillas being in the $|0\rangle$ state to compute the actual value of $\sigma_{\min}^* \|A^+ |b\rangle\|_2 / 2$, i.e., the amplitude of the state $|0\rangle^{\otimes a} |x\rangle$ (a formal definition of QAE is given later in Thm. 9). The basis-encoded two's complement representation of this amplitude can then be used to properly rescale computations involving $|x\rangle$. Note that for calculating $\|A^+ \vec{b}\|_2$ from $\|A^+ |b\rangle\|_2$ we can use the equality $\|A^+ \vec{b}\|_2 = \|A^+ |b\rangle\|_2 \|\vec{b}\|_2$ and the fact that $\|\vec{b}\|_2$ is necessarily known.

Remark 8 (Solving The Input Problem). Following the requirements of Cor. 2, the quantum speedup for solving SLEs with the stated algorithm relies heavily on the computational complexity of the block-encoding of A , as well as the state preparation of $|b\rangle$. While $|b\rangle$ can straightforwardly be prepared in time logarithmic to the dimensions of the SLE via Lem. 3 at the cost of linearly many ancillaries, the block-encoding of A is more intricate. The tool we will use to accomplish this for arbitrary sparse matrices is the block-encoding technique for sparse-access matrices described in Lem. 6. When the matrix is particularly structured, significantly more

efficient alternative block-encodings might be possible (cf. [25]). The main insight facilitating our approach is that the necessary oracles can be implemented using the controlled quantum state preparation routine of Thm. 2. For any A of dimensions $\leq N = 2^n$, this idea yields $(\sqrt{s_r s_c} \sigma_{\max}^*, n + 3, \varepsilon_1 + \varepsilon_2)$ -block-encoding of A of depth $\mathcal{O}(\log(N) + \log(1/\varepsilon_1) + \log^{2.5}(s_r s_c / \varepsilon_2))$ while requiring $\mathcal{O}(N + 1/\varepsilon_1 + \log^{2.5}(s_r s_c / \varepsilon_2))$ ancillary qubits. Here, $\lceil \log_2 1/\varepsilon_1 \rceil \in \mathbb{N}$ represents the number of bits needed for an ε_1 -approximation of the binary representation of the matrix entries of the block-encoding a_{ij} / σ_{\max}^* , so that $1/\varepsilon_1 = \mathcal{O}(\min_{ij} (|a_{ij}|) / \sigma_{\max}^*)$ if we assume the desired accuracy for even the smallest entry (e.g. 10^{-7} for single precision or 10^{-16} for double precision) as a fixed value corresponding to the multiplicative constant hidden in the \mathcal{O} -notation. This approach results in a quantum linear system solver of depth $\tilde{\mathcal{O}}(\log(N) \sqrt{s_r s_c} \kappa^* \log(\kappa^* \sqrt{s_r s_c} / \varepsilon_3) \log(1/\varepsilon_1))$, $\mathcal{O}(n)$ working qubits and $\tilde{\mathcal{O}}(N + 1/\varepsilon_1)$ ancillaries to produce an $\mathcal{O}(\varepsilon_1 + \varepsilon_2 + \varepsilon_3)$ -approximation of $|x\rangle$ that can be post-selected with success probability $\Omega((\kappa^* \sqrt{s_r s_c})^2)$, where ε_3 denotes the accuracy of the inversion polynomial.

E. Amplitude Arithmetic

In this section, we will address non-linear amplitude transformations as in $|\psi\rangle = \sum_{j=0}^{2^n-1} \alpha_j |j\rangle \mapsto 1/\mathcal{N} \sum_{j=0}^{2^n-1} f(\alpha_j) |j\rangle$, for polynomially approximable functions $f \in \mathbb{R}[x]$, where \mathcal{N} denotes the corresponding normalization factor. This allows for non-linear post

processing steps for the output of the simulation problem.

Theorem 6 (Diagonal block-encoding of state vectors [62, Thm. 2]). *Given access to an n -qubit unitary $U : |0\rangle^{\otimes n} \mapsto |\psi\rangle$, the quantum circuit in Fig. 4 implements a $(1, n+2, 0)$ -block-encoding of the diagonal matrix $\text{diag}(\text{Re}(|\psi\rangle))$ in circuit depth $\mathcal{O}(n)$ and $\mathcal{O}(1)$ queries of a controlled- U gate for $p = 0$. The circuit can alternatively block-encode the imaginary part of $|\psi\rangle$ when setting $p = 1$.*

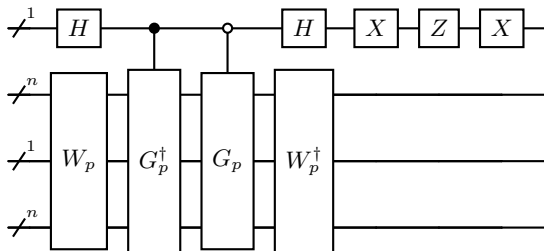


FIG. 4. Quantum circuit implementing a $(1, n+2, 0)$ -block-encoding of the diagonal matrix $\text{diag}(\text{Re}(|\psi\rangle))$ as defined in Thm. 6. Implementations for the operators G_p and W_p are displayed in Fig. 11 and Fig. 12 in the Appendix.

Theorem 7 (Non-linear amplitude arithmetic [62, Thm. 4]). *Given access to an n -qubit unitary $U : |0\rangle^{\otimes n} \mapsto |\psi\rangle \in \mathbb{R}^{2^n}$, we can prepare an ε -approximation of $f(|\psi\rangle)/\mathcal{N}$ for any given $f \in \mathbb{R}[x]$ satisfying $f(0) = 0$, for which a degree $k = K(\varepsilon\mathcal{N}^2/\gamma 2^n)$ polynomial $P \in \mathbb{R}[x]$ exists, that $\frac{\gamma 2^n}{\varepsilon\mathcal{N}^2}$ -approximates f with $P(0) = 0$, where $\gamma := \max_{-1 \leq x \leq 1} |f(x)|$, $\mathcal{N}^2 := \|f(|\psi\rangle)\|_2$, and K denotes a function describing the degree of the polynomial in terms of the error. This can be done at arbitrarily high success probability, $\mathcal{O}(\tilde{\gamma}k/\mathcal{N})$ query complexity, an overall circuit depth of $\mathcal{O}(n\tilde{\gamma}k/\mathcal{N})$ and using $\mathcal{O}(n)$ ancillas, where $\tilde{\gamma} := \max_{-1 \leq x \leq 1} |P(x)/x|$.*

F. Data readout

In this section we present different subroutines that allow us to retrieve summary statistic information from an n -qubit quantum state $|\psi\rangle$ given its state preparation unitary $U : |0\rangle^{\otimes n} \mapsto |\psi\rangle$.

Theorem 8 (Quantum Phase Estimation [63] and [64, Appendix C]). *Given an n -qubit unitary operator U and a corresponding eigenvector $|\psi\rangle$ s.t. $U|\psi\rangle = e^{2\pi i\theta}|\psi\rangle$ and $\text{wlog } \theta \in [-0.5, 0.5]$, we can compute a basis-encoded ε -approximation of θ with success probability $1 - \delta$ for any $0 < \delta < 1$ in a quantum circuit of query complexity $\mathcal{O}(1/\varepsilon\delta)$ using $n + (m + \lceil \log_2(1/2\delta + 1/2) \rceil)$ qubits with $m := \lceil \log_2(1/\varepsilon) \rceil$. The additive time complexity on top of the stated query complexity is $1 + (\lceil \log_2(1/\varepsilon) \rceil + \lceil \log_2(1/2\delta + 1/2) \rceil)^2$.*

Remark 9. The key for achieving the success probability of $1 - \delta$, is doing a standard QPE involving all ancillary qubits, but then only using the result of the $\lceil \log_2(1/\varepsilon) \rceil$ most significant bits.

Theorem 9 (Quantum Amplitude Estimation [65, Thm. 12]). *Given an n -qubit unitary operator $\mathcal{A} : |0\rangle^{\otimes n} \mapsto |\psi\rangle := e^{i\varphi} \cos\theta |\psi_0\rangle + \sin\theta |\psi_1\rangle$ with $-\pi/2 \leq \theta \leq \pi/2$, we can compute a basis-encoded $(\varepsilon_1 + \varepsilon_2)$ -approximation of $|\sin\theta|$ with success probability $1 - \delta$ for any $0 < \delta < 1$ by applying QPE on $|\psi\rangle$ and $\mathcal{Q} := -\mathcal{A}U_0\mathcal{A}^\dagger U_{\psi_1}$, where $U_0 := \mathbb{I} - 2|0\rangle^{\otimes n}\langle 0|^{\otimes n}$ and $U_{\psi_1} := \mathbb{I} - 2|\psi_1\rangle\langle\psi_1|$, and arithmetically post-processing the result with the function $\sin(\pi|\cdot|)$. Here ε_2 denotes the error of a polynomial approximation of the $\sin(\pi|\cdot|)$ function. Note that as the computational overhead of this arithmetic operation is fairly small in practice, we assume it to be constant in the rest of this paper for the sake of readability.*

Proof. Applying QPE on the specified operator \mathcal{Q} with the initial state $|\psi\rangle$ prepared using the given operator \mathcal{A} , yields an ε_1 -approximation of $i/\sqrt{2}(e^{i\theta}|\theta_-\rangle|\psi_-\rangle - e^{-i\theta}|\theta_+\rangle|\psi_+\rangle)$, where $\theta_\pm := \pm\theta/\pi$ is encoded in twos-complement representation and $|\psi_\pm\rangle := 1/\sqrt{2}(|\psi_1\rangle \pm i|\psi_0\rangle)$. Using the well-known procedure to flip the sign of a bit string encoded in twos-complement (i.e., flipping all bits and then adding one) conditionally for $|\theta_-\rangle$ via an extra ancilla, one can perform the absolute value function. For executing the $z \mapsto \sin(\pi z)$ function, we employ a truncated series approximation of degree d via Lem. 4 which introduces an error $\varepsilon_2 = \mathcal{O}(1/d!)$ additively on top of ε_1 . \square

Remark 10. Perhaps the most common application of QAE involves the estimation of a single amplitude of $|\psi\rangle$, i.e., $\psi_1 \in \{0, 1\}^n$. In this case, U_{ψ_1} can be implemented as a multi-controlled Z -gate sandwiched with an X - or I -gate on every i -th qubit, depending on whether the i -th bit of ψ_1 is 1 or 0 respectively. Note that the negative sign in \mathcal{Q} can, e.g., be implemented by the gate sequence $I^{\otimes n-1} \otimes XZXZ$, which becomes necessary, as QPE applies \mathcal{Q} as a controlled gate, s.t. its global phase matters.

Lemma 7 (Expectation Value via Hadamard Test [66]). *Given $|\psi\rangle$ via $U : |0\rangle^{\otimes n} \mapsto |\psi\rangle$, we can compute an $(\varepsilon_1 + \varepsilon_2)$ -approximation of $\langle\psi|H|\psi\rangle$ with success probability $1 - \delta$ for any $0 < \delta < 1$ by applying QAE on $\mathcal{Q} := \mathcal{A}U_0\mathcal{A}^\dagger U_{\psi_1}$, where $U_0 := \mathbb{I} - 2|0\rangle^{\otimes n}\langle 0|^{\otimes n}$, $U_{\psi_1} := Z \otimes \mathbb{I}$, and \mathcal{A} representing a Hadamard test of $|0\rangle^{\otimes m}|\psi\rangle$ with U_H , a given $(1, m, 0)$ -block-encoding of the hermitian $2^n \times 2^n$ matrix H . A quantum circuit implementing \mathcal{Q} is displayed in Fig. 5.*

Proof. Analog to Thm. 9, QPE yields a basis encoded superposition of $\pm 1/\pi \arcsin(\sqrt{1/2 + \langle\psi|H|\psi\rangle/2})$ in twos-complement representation. Following the same steps as in the proof of Thm. 9 for computing the function $z \mapsto \sin(\pi|z|)$, we then have to subsequently compute $z \mapsto 2(z^2 - 1/2)$, again by first computing the inner part

by squaring z , then subtracting $1/2$ and finally multiplying by 2. The error dependence is analog to Thm. 9. \square

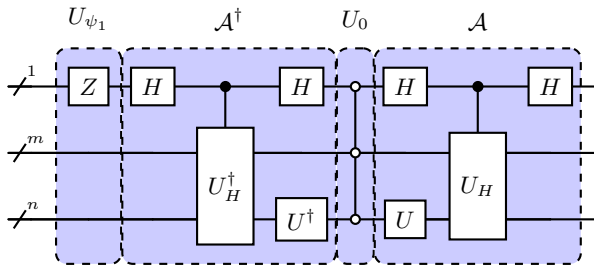


FIG. 5. Quantum circuit implementing \mathcal{Q} from Lem. 7.

Corollary 3 (Fidelity via Hadamard Test [66]). *Given $U_\psi : |0\rangle^{\otimes n} \mapsto |\psi\rangle$ and $U_\varphi : |0\rangle^{\otimes n} \mapsto |\varphi\rangle$, we can compute an $(\varepsilon_1 + \varepsilon_2)$ -approximation of $|\langle\varphi|\psi\rangle|$ with success probability $1 - \delta$ for any $0 < \delta < 1$ by applying the algorithm proposed in Lem. 7 to $m = 0$, $U = I^{\otimes n}$ and $U_H := U_\varphi^\dagger U_\psi$.*

Proof. Analog to Lem. 7, QAE for the specified inputs yields $\pm 1/\pi \arcsin(\sqrt{1/2 + |\langle\varphi|\psi\rangle|/2})$. The rest of the proof is completely analog to the one of Lem. 7. \square

Remark 11. If one only has access to an oracle preparing a state $|\psi'\rangle = \sin\theta |0\rangle^{\otimes m} |\psi\rangle + e^{i\varphi} \cos\theta |*\rangle |*\rangle$ instead of $|0\rangle^{\otimes m} |\psi\rangle$, Lem. 7 and Cor. 3 can be applied nevertheless by adding $-Z$ -gates to each non-zero qubit of the m -qubit register in the U_{ψ_1} operator.

III. METHODOLOGY

In this section, we present a framework of quantum algorithms to solve LinQuSO problems. The general setup consists of the QAOA being used to solve the optimization, the QSVT for solving the SLE and the QPE for extracting summary statistic information. We start by proposing a straightforward quantum algorithm that allows for constructing the cost unitary $|x\rangle \mapsto e^{-i\gamma_i f(x)}$ given access to the circuit computing the summary statistic result of the simulation problem $\text{QSim } |x\rangle |0\rangle^{\otimes m} = |x\rangle |u(s(x))\rangle$ to integrate the simulation component into the QAOA.

Lemma 8 (Quantum Phase Application). *Given a number $a \in \mathbb{R}$ in an encoding of the form $\sum_{i=1}^m \alpha_i a_i$, where $\alpha_i \in \mathbb{R}$ and $a_i \in \{0, 1\}$ for all $i \in [m]$, we can implement $U_c : |a\rangle \mapsto e^{-i\gamma a} |a\rangle$ for any $\gamma \in \mathbb{R}$ via the depth-1 layer of phase gates $\bigotimes_{i=1}^m P(-\gamma \alpha_i)$.*

Proof. The result directly follows from the definition of the phase gate, as $(\bigotimes_{i=1}^m P(-\gamma \alpha_i)) |a\rangle = \bigotimes_{i=1}^m P(-\gamma \alpha_i) |a_i\rangle = e^{-i\gamma \sum_i \alpha_i a_i} |a\rangle = e^{-i\gamma a} |a\rangle$. Note however, that γ has to be chosen small enough wrt. a , if the conducted phase application should be injective. \square

For simplicity, we initially assume that the QuSO problem is already binary, unconstrained, and that its costs are already fully determined by the simulation problem, i.e., $f(x) = u(s(x))$. Possible generalizations are shown subsequently.

Theorem 10 (QuSO Solver Architecture). *Given a quantum circuit implementing $\text{QSim } |x\rangle |0\rangle^{\otimes m} = |x\rangle |u(s(x))\rangle$, we can implement the cost unitary $U_C(\gamma_i) |x\rangle = e^{-i\gamma_i u(s(x))} |x\rangle$ using m ancillary qubits, one application of QSim, the quantum phase application (QPA) as proposed in Lem. 8, and one application of QSim^\dagger . Given user-specifiable oracles for the initial state preparation U_S (e.g., $H^{\otimes n}$) and a mixer unitary (e.g., $R_X(-\beta_i)^{\otimes n}$), we can construct a quantum circuit implementing the QAOA for finding $\arg \min_x u(s(x))$. For computing the costs of the final output (which is assumed to be severely less efficient classically), we add an application of QSim directly before the measurement to yield these costs. The complete circuit is displayed in Fig. 6. For the sake of simplicity, we excluded a rescaling component from this construction, which could however be straightforwardly added via the implementation stated in Rem. 7.*

Proof. The following calculation proves that our implementation of the cost unitary is correct.

$$\begin{aligned} & \text{QSim}^\dagger (I^{\otimes n} \otimes \text{QPA}(\alpha, \gamma_i)) \text{QSim } |x\rangle |0\rangle^{\otimes m} \\ &= \text{QSim}^\dagger (I^{\otimes n} |x\rangle \otimes \text{QPA}(\alpha, \gamma_i) |u(s(x))\rangle) \\ &= \text{QSim}^\dagger e^{-i\gamma_i u(s(x))} |x\rangle |u(s(x))\rangle \\ &= e^{-i\gamma_i u(s(x))} |x\rangle |0\rangle^{\otimes m} \end{aligned}$$

As the rest of our implementation besides the extra measurement of $|u(s(x))\rangle$ is analog to a standard QAOA procedure (cf. Thm. 1), this completes the proof. \square

We now discuss how more general QuSO problems than the minimal form of $\arg \min_x u(s(x))$ can be solved by extending the circuit structure presented in Thm. 10.

Remark 12 (Solving Mixed-Integer QuSO problems). As typical for any quantum optimization algorithm based on identifying the optimization problems' cost landscape with the energy spectrum of a Hamiltonian, we also have to resort to an appropriate, problem-dependent discretization of all continuous decision variables.

Remark 13 (Integrating arbitrary continuous cost functions). As a corollary of Rem. 12, the domain space of the decision variables is necessarily bounded. By defining a closed interval that contains this reduced domain space, we can make use of the Stone–Weierstrass theorem [67] to find a polynomial approximation of the cost function f . This polynomial can be translated into an Ising Hamiltonian (cf., e.g., [68]) so that the value of the specific function can be computed in basis encoding using Lem. 7. The summary statistic result of the simulation problem $u(s(x))$ can then be integrated into the rest

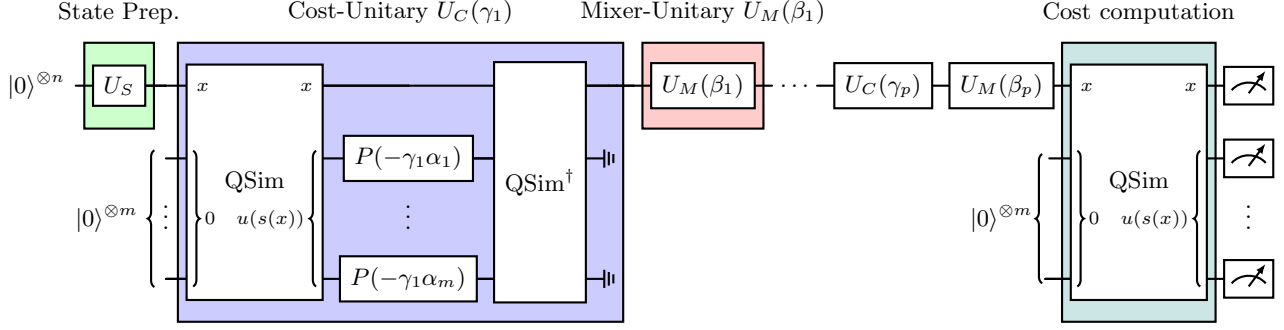


FIG. 6. Quantum circuit solving a QuSO problem of the form $\arg \min_x f(x) = u(s(x))$ as proposed in Thm. 10. A potential implementation for QSim can be found in Fig. 9. The \parallel symbol is used to mark ancillas in the $|0\rangle$ state that can be reused for further calculations.

of $f(x)$ via the QSim operator corresponding to $u(s(x))$ and quantum arithmetic operations. In the special case where $u(s(x))$ is just an additive term in $f(x)$, one can simply append the cost unitary corresponding to $u(s(x))$ to any previous cost unitaries of other terms of $f(x)$ in the quantum circuit, as all cost operators commute.

Remark 14 (Integrating constraints into the QuSO solver). One possibility of integrating constraints in the QuSO solver architecture of Thm. 10 is via the introduction of penalty terms. This way, we can exploit the same approach as in Rem. 13. Details about the general approach to formulate constraints as penalty terms can be found in Sec. II B

Having shown concrete techniques for solving general QuSO problems, we now focus on the implementation of QSim for a large class of LinQuSO problems. In particular, we prove that this approach allows for exploiting exponential quantum speedup for the simulation component. An overview of the framework of quantum algorithms we provide for implementing QSim is given in Table I in the Appendix.

A. Data input

In this section, we show how the controlled quantum state preparation algorithm from Thm. 2 can be adapted to implement the quantum data input necessary for solving a decision variable dependent SLE $A_x \vec{y} = \vec{b}_x$ with the QSVT. The notation with the binary decision variables $x \in \{0, 1\}^n$ as a subscript to A and \vec{b} denotes that their entries depend on x . We now show how to efficiently prepare \vec{b}_x and block-encode A_x depending on their dependence on x .

Lemma 9 (Fast controlled State Preparation). *Given a fixed $x \in \{0, 1\}^m$ and a normalized vector $\vec{b}_x \in \mathbb{R}^{2^n}$ with entries of arbitrary form, i.e., $(\vec{b}_x)_i = b(x)_i$ for all $x \in \{0, 1\}^m$ and $i \in [N]$ for arbitrary functions $b: \{0, 1\}^m \rightarrow \mathbb{R}^{2^n}$, we can implement a state preparation of \vec{b}_x with a circuit of depth $\mathcal{O}(n)$ using $\mathcal{O}(N2^m)$ ancillary qubits.*

Proof. By applying Thm. 2 to execute $|x\rangle |0\rangle^{\otimes n} \mapsto |x\rangle |b_x\rangle$ one directly gets the stated complexities. \square

In practice, the function $b(x)$ from Lem. 9 is usually less arbitrary, which can allow for exponentially better space requirements as shown in Thm. 11.

Theorem 11 (Quantum Digital to Analog Conversion for Bitstrings). *Given an n -qubit computational basis state $|x\rangle$ with $n = 2^\eta$ for some $\eta \in \mathbb{N}$ and a state preparation oracle $U_c: |0\rangle^\eta \mapsto |c\rangle$, we can perform $|x\rangle |0\rangle |0\rangle^{\otimes \eta} \mapsto |x\rangle (|0\rangle \sum_i^\eta c_i x_{k(i)} |i\rangle + |1\rangle \sum_i^\eta c_i (1 - x_{k(i)}) |i\rangle)$ using a quantum circuit of depth $\mathcal{O}(\log n)$ and $\mathcal{O}(n^2)$ ancillary qubits, where $k: [n] \rightarrow [n]$ maps every index of $|c\rangle$ to an index of $|x\rangle$.*

Proof. A naive setup for constructing a circuit that allows for implementing the specified operator with $k(i) = i$ is displayed in Fig. 7. As evident by the circuit construction, the core operation of the circuit is the $(\eta, n+1)$ -UCU with U_i defined as a controlled not gate with the target being fixed on the ancillary qubit and the target being on the $k(i)$ -th qubit of the $|x\rangle$ register. Through an equivalent reformulation of this circuit, we convert the stated UCU into a much less complex UCU that allows the application of Lem. 10 from Ref. [27] to implement this UCU⁵. For the reformulation, we use these two tricks: (1) control and target of a controlled not gate can be switched by a Hadamard sandwich, and (2) a controlled gate can be constructed via a sandwich of controlled swap operators (cf. [59, Fig. 5]). This yields the circuit displayed in Fig. 8, which clearly allows the application of Lem. 10 from Ref. [27] and hence yields the unitary operator specified in the theorem with the stated complexities up to the implementation of the controlled swap gates. As the controlled swap gates on both sides result in permutation matrices, we employ Lem. 10 to complete the proof. \square

⁵ Note that the necessary conditions for Lem. 11 from Ref. [27] are not satisfied in the construction of Fig. 7, as the U_i operators do not fulfill the property of being a standard quantum circuit.

Corollary 4. *Thm. 11 can be generalized to η being independent of n by adapting the employed (n, η) -UCU with $k : [2^n] \rightarrow [n]$ while keeping $U_i = X_{k(i)}$. Using the same proof structure as in Thm. 11, this generalization yields a circuit depth of $\mathcal{O}(\log n + \log N)$ and requires $\mathcal{O}(nN)$ ancillary qubits for $b_x \in \mathbb{R}^N$ for an n -qubit computational basis state $|x\rangle$.*

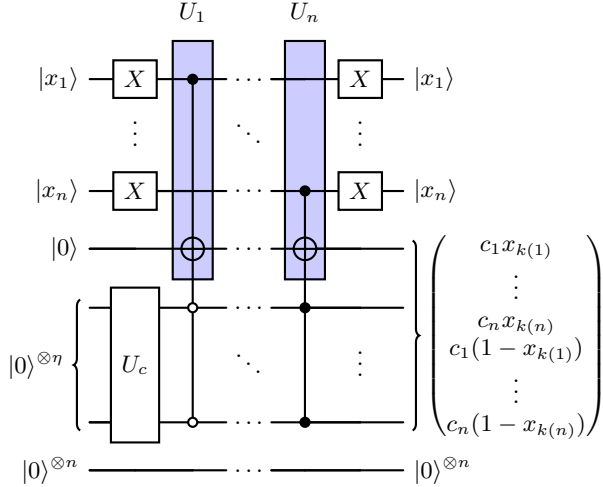


FIG. 7. Quantum circuit for QDAC with bitstrings as shown in Thm. 11 for $k(i) = i$. The uniformly controlled unitary can be constructed efficiently using [27, Lem. 10] on the UCU of the standard quantum circuit shown in Fig. 8.

Lemma 10 (Fast Permutation Operators). *Given a sequence of n swap operations $S_i := \text{SWAP}(j_i, k_i)$ on n qubits with $j_i, k_i \in [n] \forall i \in [n]$, we can implement the resulting unitary operator $\prod_i S_{i \in [n]}$ in depth $\mathcal{O}(\log n)$ using $\mathcal{O}(1)$ ancillary qubits.*

Proof. We can classically precompute the resulting permutation in $\mathcal{O}(n)$ steps and then use Lem. 6 together with Thm. 2 to achieve the stated complexity. As the block-encoded matrix is unitary, no post-selection is necessary. \square

We now continue by showing how to accomplish similar complexities for matrix block-encoding. For that, we start with the baseline of block-encoding a matrix independent of any decision variables by formalizing Rem. 8.

Lemma 11 (Fast Block-Encoding). *Given an s_r -row- and s_c -column-sparse matrix $A \in \mathbb{R}^{2^n \times 2^n}$ as well as an upper bound σ_{\max}^* on its maximal singular value, we can implement a $(\sqrt{s_r s_c} \sigma_{\max}^*, n + 3, \varepsilon_1 + \varepsilon_2)$ -block-encoding of A with circuit depth $\tilde{\mathcal{O}}(n)$ using $\tilde{\mathcal{O}}(N + \log 1/\varepsilon_1)$ ancillary qubits, where $1/\varepsilon_1 = \mathcal{O}(\sigma_{\max}^* / \min_{ij} |a_{ij}|)$.*

Proof. We use the general circuit architecture of Lem. 6 and Thm. 2 for implementing each oracle to yield the desired unitary operator with the stated complexities. \square

Lemma 12 (Fast controlled Block-Encoding). *Given $A_x \in \mathbb{R}^{2^n \times 2^n}$ with s_r denoting the minimal row- and s_c the minimal-column-sparsity of A_x over all x as well as an upper bound σ_{\max}^* on the maximal singular value of all A_x , we can implement a $(\sqrt{s_r s_c} \sigma_{\max}^*, n + 3, \varepsilon_1 + \varepsilon_2)$ -block-encoding of A_x for every $x \in \{0, 1\}^m$ with circuit depth $\tilde{\mathcal{O}}(n)$ using $\mathcal{O}(N 2^m + \log 1/\varepsilon_1)$ ancillary qubits where $1/\varepsilon_1 = \mathcal{O}(\sigma_{\max}^* / \min_{ij} |a_{ij}|)$.*

Proof. Analog to Lem. 9, we use the general circuit architecture of Lem. 6 and Thm. 2 for implementing each oracle, however, to account for the fact that the oracles are now dependent on x , we have to extend the control register in Thm. 2 to include x which yields the increased complexity. \square

Theorem 12 (Optimal controlled block-encoding). *Given $A_x \in \mathbb{R}^{2^n \times 2^n}$ with s_r denoting the minimal row- and s_c the minimal-column-sparsity of A_x over all x with entries of the form $a_{ij} x_{k(i,j)}$ where $k : [n]^2 \rightarrow [m]$ maps every entry index of A to an index of x , as well as an upper bound σ_{\max}^* on the maximal singular value of all A_x , we can implement a $(\sqrt{s_r s_c} \sigma_{\max}^*, n + 3, \varepsilon_1 + \varepsilon_2)$ -block-encoding of A_x for every x with circuit depth $\tilde{\mathcal{O}}(n)$ using $\mathcal{O}(Nm + \log 1/\varepsilon_1)$ ancillary qubits where $1/\varepsilon_1 = \mathcal{O}(\sigma_{\max}^* / \min_{ij} |a_{ij}|)$.*

Proof. The exponentially reduced space complexity in m can be achieved by a similar setup as in Thm. 11. More concretely, we start with our typically employed block-encoding from Lem. 11 for a matrix with entries a_{ij} but stop before the AQE step. Before conducting the AQE and O_A^\dagger , we insert the UCU from Thm. 11 controlled on the matrix index registers to compute the value of the respective $x_{k(i,j)}$ on the ancillary qubit. Then we control the AQE on this ancilla to make sure that the value for a_{ij} is only respected if the corresponding $x_{k(i,j)}$ equals one. After that, we uncompute this step (except for the AQE) to then finally uncompute O_A to finish the block-encoding. By applying the implementation setup from Fig. 8 for the UCU, we end up with an algorithm of the stated complexity. \square

B. Amplitude Arithmetic

In this section, we show an upper bound on the complexity of performing the absolute value function on quantum amplitudes as an addendum to list of non-linear amplitude manipulation functions proposed in Thm. 5 of Ref. [62].

Lemma 13 (Approximating $|\cdot|$). *Given access to an n -qubit unitary $U : |0\rangle^{\otimes n} \mapsto |\psi\rangle \in \mathbb{R}^{2^n}$, we can implement an ε -approximation of state preparation unitary for $||\psi\rangle\rangle$ via Thm. 7 using the polynomial*

$$P(x) = \frac{2}{\pi} + \frac{4}{\pi} \sum_{k=1}^d \frac{(-1)^{k+1}}{4k^2 - 1} T_{2k}(x), \quad (6)$$

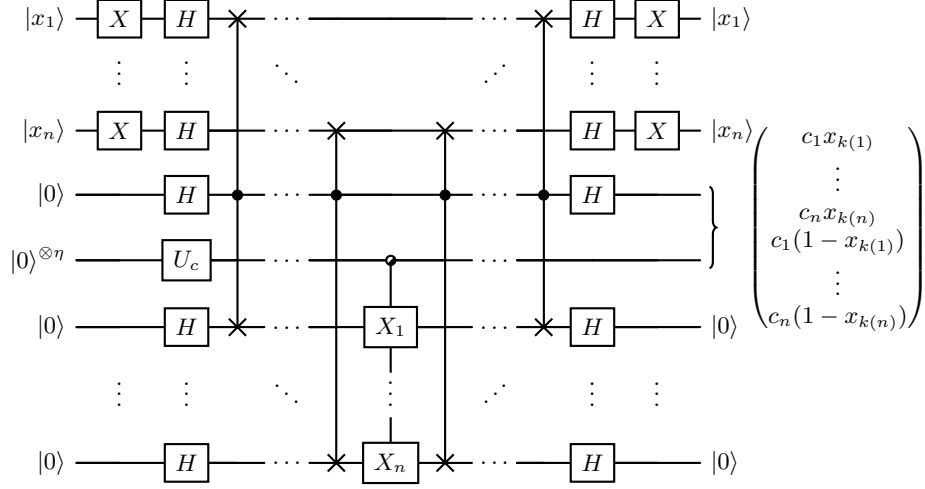


FIG. 8. Standard quantum circuit realizing Thm. 11 for $k(i) = i$. $X_{k(i)}$ is chosen to be the X -gate only for the control being the bitstring $i - 1$, otherwise it is asserted to the identity gate. For $k(i) \neq i$, the swaps have to be carried out on the $k(i)$ -th qubits of the top and bottom registers.

where $T_k(x)$ denotes the k -th Chebychev polynomial of the first kind and $d = \mathcal{O}(\lceil 1/\pi\varepsilon \rceil)$. The query complexity in U is $\mathcal{O}(d)$ and the overall circuit depth is $\mathcal{O}(nd)$ with $\mathcal{O}(n)$ needed ancillas. The classical overhead cost for computing the circuit is $\mathcal{O}(\text{polylog}(2^n/\varepsilon^2))$.

Proof. Based on the proof of the approximation accuracy of P (outsourced to the Appendix in Lem. 24), we can use Thm. 7 to yield the stated complexities. \square

C. Assembling QSim

In this section, we present an approach to solve SLEs of the form $A_x \vec{y} = \vec{b}_x$ using the QSVT in practice. Further, we show how to extract specific summary statistic information from the resulting SLE result, to yield a concrete implementation of the QSim operator specified in Thm. 10.

Corollary 5 (Quantum SLE solver for $A_x \vec{y} = \vec{b}_x$). *Given a system of linear equations of the form $A_x \vec{y} = \vec{b}_x$ with s_r denoting the minimal row- and s_c the minimal-column-sparsity of A_x over all x with entries of the form $a_{ij} x_{k(i,j)}$ where $k : [n]^2 \rightarrow [m]$ maps every entry index of A to an index of x , as well as an upper bound σ_{\max}^* on the maximal singular value of all A_x , a lower bound $\sigma_{\min}^* > 0$ on the minimal non-zero singular values of all A_x , and b_x with entries of the form $b_i x_{k(i)}$ for all x , then we can compute a rescaled version of $\vec{y} = A_x^+ \vec{b}_x$ in a circuit of depth $\tilde{\mathcal{O}}(\text{polylog}(N)\kappa^* \sqrt{s_r s_c})$ using $\tilde{\mathcal{O}}(N^2)$ ancillary qubits.*

Lemma 14 (Rescaling the quantum SLE solvers output). *Given a quantum linear systems solver that aims to compute $|y\rangle = A_x^+ \vec{b} / \|A_x^+ \vec{b}\|_2$, i.e., a rescaled version of the actual result $\vec{y} = A^+ \vec{b}$. As evident by Rem. 8, the*

subnormalization factor induced by the block-encoding of A_x is of order $\mathcal{O}(\sigma_{\max}^* \sqrt{s_r s_c})$. We can then use Quantum Amplitude Estimation as described in Thm. 9 on the state of the ancillas being in the $|0\rangle$ state to compute the actual value of $\sigma_{\max}^* \sqrt{s_r s_c} \|A^+ |b\rangle\|_2 / 2$, i.e., the amplitude of the state $|0\rangle^{\otimes a} |x\rangle$. The basis-encoded two's complement representation of this amplitude can then be used to properly rescale computations involving $|x\rangle$. Note that for calculating $\|A^+ \vec{b}\|_2$ from $\|A^+ |b\rangle\|_2$ we can use the equality $\|A^+ \vec{b}\|_2 = \|A^+ |b\rangle\|_2 \|\vec{b}\|_2$ and the fact that $\|\vec{b}\|_2$, σ_{\max}^* and $\sqrt{s_r s_c}$ are necessarily known.

Theorem 13 (Assembling QSim). *We can implement a quantum circuit computing $\text{QSim}[x] |0\rangle^{\otimes m} = |x\rangle |u_j(s(x))\rangle$ for any $j \in [3]$ and $s : x \mapsto A_x^+ b_x$ and $u_1 : y \mapsto y_i$, $u_2 : y \mapsto \langle y, z \rangle$, $u_3 : y \mapsto y^\top H y$ for a given state preparation of z and block-encoding of H , where s represents an SLE of which we are given what is also assumed in Cor. 5 in a circuit of depth $\tilde{\mathcal{O}}(\text{polylog}(N)\kappa^* \sqrt{s_r s_c} / \varepsilon \delta)$ using $\tilde{\mathcal{O}}(N^2)$ ancillary qubits where ε denotes the QAE accuracy and $0 < \delta < 1$ the success probability of QAE. An example circuit for u_1 is shown in Fig. 9.*

Proof. We use Cor. 5 to implement the SLE solver and Thm. 9 for u_1 , Cor. 3 for u_2 , and Lem. 7 for u_3 to compute the rescaled version of $|u(s(x))\rangle$. To fix the scaling, we run Lem. 14 with a separate ancillary register to compute the rescaling factor, which is then used in a quantum arithmetic step to compute $|u(s(x))\rangle$. \square

IV. EXAMPLES

In this section, we show how two industrial applications (one from the energy sector and one from structural

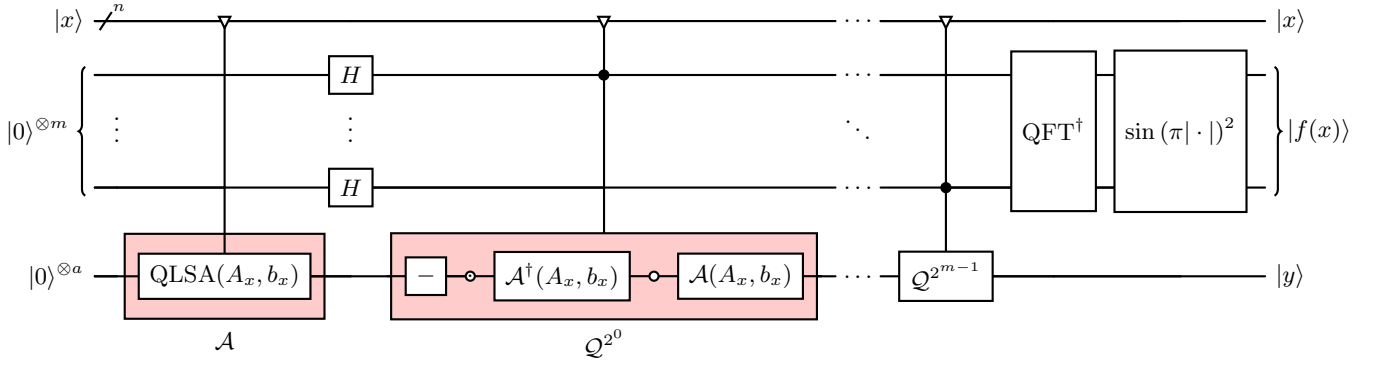


FIG. 9. Quantum circuit implementing QSim from Fig. 6 when the summary statistic information of interest is stored in a single amplitude (cf. Thm. 9). $\text{QLSA}(A_x, b_x)$ denotes a quantum linear system algorithm for the SLE $A_x \vec{y} = \vec{b}_x$ (cf. Cor. 2). The \circ symbol denotes a controlled Z-gate with the control of a subset of wires actuating upon $|0\rangle$ instead of $|1\rangle$. The ∇ symbol denotes specific control operators representing the controls in Fig. 7 although the required QDAC is implemented via the circuit in Fig. 8.

engineering) can be formulated as QuSO problems and how our methodology allows up to exponential quantum speedups to solve them.

A. Unit Commitment

As an example for an SLE with the structure $A\vec{y} = \vec{b}_x$, and an application of Thm. 11 (and Cor. 4 respectively), we now show how a highly relevant problem from industry (i.e., the unit commitment problem) can be formulated as a LinQuSO problem and identify that it can be solved via Thm. 10 and Thm. 13. The unit commitment problem is a MINLP-type optimization problem that concerns the amount of power that is generated at each power generator in a power grid to provide enough power for an estimated demand at the lowest cost. The simulation problem that contributes to the costs is called the power flow problem, which concerns the calculation of the amount of power flowing through every transmission line $\vec{\rho}$, given the power in- and outputs at each node (also called bus) in the power grid p_i . The cost that typically needs to be extracted from the result of the power flow problem is of the form $|\langle \vec{c}, \vec{\rho}_x \rangle|$, where \vec{c} denotes the linear cost factor to transmit power over each transmission line. While the unit commitment problem has many other cost factors and constraints (that could be incorporated into our QuSO solver as described in Rems. 12 to 13), we will focus on a reduced form of it which only considers the power flow and the costs resulting from it. More specifically, we investigate a specific but very common linear approximation of AC power flow, the DC power flow approximation.

To simplify the definition of the exact form of the unit commitment problem that we want to investigate, we now introduce some notation together with a well-known result from graph theory.

Lemma 15. *Given the Laplacian matrix \mathcal{L} of an N -node*

graph \mathcal{G} , every cofactor $\mathcal{L} := \mathcal{L}[i]$ (i.e., the matrix that results when the i -th row and i -th column are removed from \mathcal{L} , where $i \in [N]$) is invertible.

Proof. By the matrix tree theorem [69], the determinant of all cofactors is equal to the number of spanning trees of \mathcal{G} , and by Kirchhoff's theorem [70], this number is equal to the product of all non-zero eigenvalues of \mathcal{L} divided by N . \square

Definition 7 (Power flow focused unit commitment). *Given a power grid in form of a graph $\mathcal{G} = (V, E)$ of its transmission lines weighted by their susceptances $\vec{b}_{ij} \in \mathbb{R}$, $V = \{1, \dots, N\}$, a fixed value how much power $\vec{p}_i \in \mathbb{R}$ is generated or consumed (in this case, $\vec{p}_i \in \mathbb{R}^-$) by each generator $i \in G = \{1, \dots, M\} \subset V$ and load $i \in L := V \setminus G$, a reference bus $r \in V$ (wlog. $r = N$), as well as fixed values for the linear cost factor of using each transmission line $\vec{c}_{ij} \in \mathbb{R}$, then we define the problem of power flow focused unit commitment by $\arg \min_x \langle \vec{c}, |\vec{\rho}_x| \rangle$ s.t. $\sum_i \vec{p}_x \approx 0$, i.e., optimizing which generators $G_x := \{i \in G : x_i = 1\}$ should be operating to minimize the overall power transmission costs using the decision variables $x \in \{0, 1\}^M$ while the net power input is roughly equal to the net power output. Here, $\vec{\rho}_x := B' \Pi \mathcal{B}^{-1} \vec{p}_x$ denotes the power flowing over all transmission lines, where \vec{p}_x is the reduced form of the power in-/output vector \vec{p}_x (i.e., \vec{p}_x without its r -th entry), which is defined as either \vec{p}_i iff $i \in L$ or $x_i \vec{p}_i$ iff $i \in G$, further, \mathcal{B} is defined as the Laplacian matrix of \mathcal{G} with weights \vec{b}_{ij} and $\mathcal{B} := \mathcal{B}[r]$ (cf. Lem. 15). Finally, Π denotes the projection matrix mapping $\vec{\theta} := \mathcal{B}^{-1} \vec{p}_x$ onto $\vec{\theta}' := (\vec{\theta}_1, \dots, \vec{\theta}_1, \vec{\theta}_2, \dots, \vec{\theta}_2, \dots, \vec{\theta}_N, \dots, \vec{\theta}_N)$ where each $\vec{\theta}_i$ appears exactly $d_i := |\{j \in V : (i, j) \in E\}|$ often and $\vec{\theta}_r = 0$ for the chosen reference bus. Lastly, B' takes the form of an $|E| \times |E|$ dimensional matrix with diagonal entries $(\vec{b}_{1e(1,1)}, \dots, \vec{b}_{1e(1,d_1)}, \dots, \vec{b}_{Ne(N,1)}, \dots, \vec{b}_{Ne(N,d_N)})$, where a given function $e : V \times \mathbb{N} \rightarrow V$ yields the j -th neigh-*

bor of node i , and off-diagonal entries $-\vec{b}_{ie(i,k)}$ for the $(k + \sum_{\ell=1}^{i-1} \nu_\ell)$ -th row.

By $s(x) := \vec{\theta} = \mathcal{B}^{-1} \vec{p}_x$ and $u(s(x)) := \langle \vec{c}, |B'\Pi s(x)\rangle$ it becomes obvious, that Def. 7 describes a LinQuSO problem as defined in Def. 4. As this form of summary statistic information extraction is already covered by Cor. 3 and Lem. 13 up to B' and Π , the concatenation of these results can be used to implement a quantum algorithm for solving this power flow focused unit commitment problem. For the implementation of $B'\Pi$ in a quantum circuit, we can do the following: Let $d := \max_{i \in [N]} \lceil \log_2 d_i \rceil$, then $|\theta''\rangle := |\theta\rangle |+\rangle^{\otimes d}$ yields a quantum version of $\vec{\theta}'$, where $|\theta''\rangle$ is defined with the same basic structure of $\vec{\theta}'$, but with each θ_i being repeated exactly d times while also introducing the normalization factor $1/\sqrt{2^d}$ for each entry. To match this enlarged version of $\vec{\theta}'$, we have to adapt B' accordingly, i.e., adding 0-rows and -columns for each entry where $|\theta''\rangle$ exceeds $\vec{\theta}'$. The matrix resulting from this enlargement B'' can then be block-encoded via Thm. 12 analog to the block-encoding of \mathcal{B} – the only differences being the reduced sparsity (i.e., two) and the increased dimensionality (i.e., Nd). This block-encoding introduces a subnormalization factor of $4 \max_{ij} |\vec{b}_{ij}|$, which has to be taken into consideration as a rescaling factor of the result of the scalar product $\langle \vec{c}, \vec{\rho}_x \rangle$ (i.e., a rescaling factor on top of the mandatory rescaling discussed in Lem. 14). Note that the state preparation of \vec{c} also has to take the empty rows in $|\theta''\rangle$ into consideration (which the protocol of Thm. 2 easily allows for). Overall the proposed implementation of $B'\Pi$ only affects the computational complexity effectively by a constant factor as the number of ancillary qubits only increases by $\mathcal{O}(N2^d) = \mathcal{O}(Nd_{\max})$ and the QAE runtime only increases linearly with the, also basically constant, rescaling factor of $4 \max_{ij} |\vec{b}_{ij}|$.

Based off Thm. 13, the runtime of this algorithm is predominantly dependent on the condition number, as a power grid is generally quite sparse. In the following, we show how graph properties like the maximum node degree and the graph's conductance can be used to bound the condition number. Further, we show that while the condition number often scales linearly wrt. the number of nodes in real-world power grids (cf. [71]), any power grid that takes the form of a so-called expander graph has a constant condition number. In the following we focus on the eigenvalues of \mathcal{B} instead of the singular values, which is sufficient, as $\sigma_i = |\lambda_i| = \lambda_i$ for Laplacian matrices, because Laplacian matrices are always normal, and as all susceptances can be assumed to be positive (cf. Ref. [72]) [73, Thm. 4.2]).

Lemma 16 (Gershgorin circle theorem [74]). *Every eigenvalue of $A \in \mathbb{C}^{n \times n}$ lies in at least one Gershgorin disc $D_i := \{x \in \mathbb{C} : |a_{ii} + x| \leq r_i\}$, where $r_i := \sum_{j \neq i} |a_{ij}|$.*

Corollary 6. *For a graph $\mathcal{G} = (V, E)$ with edge weights $(a_{ij})_{(i,j) \in V^2} \in \mathbb{R}$ and its Laplacian matrix \mathcal{L} , the maximal eigenvalue λ_{\max} of every reduced Laplacian matrix \mathcal{L} is bound from above by $2d_{\max}$, where $d_{\max} := \max_{i \in V} d_i$ denotes its maximum degree and $d_i := \sum_{(i,j) \in E} |a_{ij}|$.*

Proof. This is a consequence of all eigenvalues of \mathcal{L} lying within the Gershgorin discs of \mathcal{L} by the Cauchy interlacing theorem [75], combined with $a_{ii} = \sum_{(i,j) \in E} a_{ij}$ and $r_i = \sum_{(i,j) \in E} |a_{ij}|$, s.t. $\lambda_{\max} \leq 2d_{\max}$. \square

Given these insights from graph theory, we can see that the largest eigenvalue of \mathcal{B} is typically reasonably small, as the maximal degree in sparse graphs hardly scales with an increasing number of nodes. This observation is also mirrored in real-world power grids (cf. [71]). Conversely, the smallest eigenvalue λ_2 can get up to quadratically small wrt. the number of nodes as $4/N \text{diam}(G) \leq \lambda_2$ as long as all susceptances are positive (which is typically the case in practice [72]) [73, Thm. 4.2]. Aiming for tighter bounds we now discuss the well-known Cheeger inequality, which will be the key for identifying the maximum possible quantum speedup for solving the power flow simulation problem as defined in Def. 7.

Definition 8 (Fiedler value). *We call the second smallest eigenvalue of a given Laplacian matrix the Fiedler value (also known as the algebraic connectivity).*

Lemma 17 (Cheeger's inequality [76]). *Given a connected graph $\mathcal{G} = (V, E)$ with edge weights $(a_{ij})_{(i,j) \in V^2} \in \mathbb{R}^+$ and its Laplacian matrix \mathcal{L} , then the conductance of \mathcal{G}*

$$\varphi(\mathcal{G}) := \min_{\substack{S \subset V \\ S \neq \emptyset}} \frac{|\partial S|}{\min(\text{vol}(S), \text{vol}(\bar{S}))} \quad (7)$$

gives lower and upper bounds to \mathcal{L} 's Fiedler value ν_2 via

$$\frac{\varphi(\mathcal{G})^2}{2} \leq \nu_2 \leq 2\varphi(\mathcal{G}), \quad (8)$$

where $\mathcal{L} := D^{-1/2} \mathcal{L} D^{-1/2}$ denotes the normalized Laplacian matrix with $D := \text{diag}(d_1, \dots, d_N)$, $|\partial S| := \sum_{i \in S} \sum_{j \in \bar{S}} a_{ij}$ denoting the weight of the edges connecting S with $\bar{S} := V \setminus S$, and $\text{vol}(S) := \sum_{i \in S} \sum_{j \in V} a_{ij}$ called the volume of S .

Lemma 18 (Relating Fiedler values of \mathcal{L} and \mathcal{L}). *Given an undirected N -node graph $\mathcal{G} = (V, E)$ with edge weights $(a_{ij})_{(i,j) \in V^2} \in \mathbb{R}^+$, its Laplacian matrix \mathcal{L} with associated Fiedler value λ_2 and its normalized Laplacian matrix \mathcal{L} with associated Fiedler value ν_2 , then:*

$$d_{\min} \nu_2 \leq \lambda_2 \leq d_{\max} \nu_2. \quad (9)$$

Proof. We only show the proof for the first inequality, as both proofs are highly analogous. First, we note that all considered matrices here are symmetric, allowing us

to form an orthonormal basis of \mathcal{L} based on the spectral theorem [77]. Due to the structure of Laplacian matrices' rows summing to zero (note that \mathfrak{L} also has the same structure), the smallest eigenvalue of \mathcal{L} as well as smallest eigenvalue of \mathfrak{L} is always 0, and their associated eigenvector from a respective orthonormal basis is $1_N := 1/\sqrt{N}(1, \dots, 1) \in \mathbb{R}^N$. Then choose w as the orthonormal basis vector associated with the second smallest eigenvalue of \mathcal{L} , i.e., $\mathcal{L}w = \lambda_2 w$ with $w^\top w = 1$ and $\langle w, 1_N \rangle = 0$. Then we can bound ν_2 via

$$\nu_2 = \min_{\substack{\langle v, 1_N \rangle = 0 \\ v \neq 0}} \frac{v^\top \mathfrak{L}v}{v^\top v} \leq \frac{w^\top \mathcal{L}w}{w^\top Dw} = \frac{\lambda_2}{\sum_i d_i w_i^2} \leq \frac{\lambda_2}{d_{\min}},$$

where the choice of $v := D^{-1/2}w$ is valid as (1) clearly $D^{-1/2}w \neq 0$ due to $w \neq 0$, and (2) $\langle D^{-1/2}w, 1_N \rangle = 0$ by $\langle D^{-1/2}w, 1_N \rangle = \sum_i w_i/\sqrt{d_i} \leq \langle w, 1_N \rangle/d_{\max} = 0$ and $\langle D^{-1/2}w, 1_N \rangle = \sum_i w_i/\sqrt{d_i} \geq \langle w, 1_N \rangle/d_{\min} = 0$. \square

Lemma 19 (Lower bound for \mathcal{L} 's λ_{\min}). *Given an undirected N -node graph $\mathcal{G} = (V, E)$ with edge weights $(a_{ij})_{(i,j) \in V^2} \in \mathbb{R}^+$, its Laplacian matrix \mathcal{L} with associated Fiedler value λ_2 and its normalized Laplacian matrix \mathfrak{L} with associated Fiedler value ν_2 , then we can provide the following lower bound on \mathcal{L} 's smallest eigenvalue λ_{\min} :*

$$\frac{d_{\min}\varphi(\mathcal{G})^2}{2} \leq d_{\min}\nu_2 \leq \lambda_2 \leq \lambda_{\min}. \quad (10)$$

Proof. The first inequality is a form of Lem. 17, the second inequality is the result of Lem. 18, and the last inequality follows from the Cauchy interlacing theorem [75], which implies that all eigenvalues of \mathcal{L} lie within the range of eigenvalues of \mathfrak{L} . \square

Having established a lower bound for the smallest eigenvalue of \mathcal{B} through Lem. 19 by means of the conductance of the underlying power grid susceptances, we now show that there exists a vast number of graphs with constant condition numbers for \mathcal{B} , i.e., so-called expander graphs and their optimal representatives: Ramanujan graphs.

Definition 9 (Expander graphs). *We call a connected graph \mathcal{G} a (d, ε) -expander iff $d_{\max} \leq d$ and $0 < \varepsilon \leq \varphi(\mathcal{G})$.*

Definition 10 (Ramanujan graphs). *We call a connected, d -regular, N -node graph $\mathcal{G} = (V, E)$ Ramanujan, iff $\lambda(\mathcal{G}) := \max_{i \neq 1} |\lambda_i| \leq 2\sqrt{d-1}$, where $\lambda_1 \geq \lambda_2 \geq \dots \geq \lambda_N$ denote the eigenvalues of \mathcal{G} 's adjacency matrix A . Note that $\lambda_1 = d$ for d -regular graphs, as every row in A sums to d such that $A1_N = d1_N$.*

Lemma 20 (Ramanujan graphs are expanders). *Every N -node d -regular Ramanujan graph is a (d, ε) -expander with $0 < \varepsilon := 1/2 - \sqrt{d-1}/d$ for $d \geq 3$.*

Proof. Combining Lem. 18 with Lem. 17 for $d_{\min} = d$ yields $\nu_2 = \lambda_2/2d \leq \varphi(\mathcal{G})$. Let w be an eigenvector of \mathcal{L} that corresponds to λ_2 (i.e., $\mathcal{L}w = \lambda_2 w$), then

$\mathcal{L}w = (d\mathbb{I} - A)w$ implies that w is also an eigenvector of A with corresponding eigenvalue $\lambda(A) := d - \lambda_2$, as $Aw = (d - \lambda_2)w$. As \mathcal{G} is connected, we have that $\lambda_2 > 0$, implying $\lambda(A) = (d - \lambda_2) \neq d$, so that we can bound $\lambda(A) \leq \lambda(\mathcal{G})$ completing the proof for the following bounds:

$$\frac{1}{2} - \frac{\sqrt{d-1}}{d} \leq \frac{d - \lambda(\mathcal{G})}{2d} \leq \frac{d - \lambda(A)}{2d} = \frac{\lambda_2}{2d} \leq \varphi(\mathcal{G}).$$

\square

Lemma 21 (Condition number of Ramanujan graphs). *The condition number of each cofactor of the Laplacian of an N -node d -regular Ramanujan graph \mathcal{L} can be bounded from above by a constant for all $d \geq 3$.*

Proof. $\lambda_{\max} \leq \lambda_{\max}^* := 2d$ is the result of Cor. 6. Further, Lems. 19 and 20 yield

$$\lambda_{\min}^* := \frac{d \left(\frac{1}{2} - \frac{\sqrt{d-1}}{d} \right)^2}{2} \leq \frac{d\varphi(\mathcal{G})^2}{2} \leq \lambda_{\min},$$

which implies the stated result via

$$\kappa^* := \frac{\lambda_{\max}^*}{\lambda_{\min}^*} = \frac{2d}{\frac{d}{2} \left(\frac{1}{2} - \frac{\sqrt{d-1}}{d} \right)^2} = \frac{4}{\left(\frac{1}{2} - \frac{\sqrt{d-1}}{d} \right)^2} = \mathcal{O}(1).$$

\square

Remark 15 (Abundance of expander graphs). While it has not yet been shown whether or not infinitely many d -regular Ramanujan graphs exist for arbitrary d , we know that there exist infinitely many d -regular Ramanujan graphs for some more specific d (e.g., $d - 1$ being a prime power [78]). When relaxing the property of being Ramanujan to weakly-Ramanujan however, i.e., $\lambda(\mathcal{G}) < 2\sqrt{d-1} + \varepsilon$ for some $\varepsilon > 0$, even widely common random d -regular graphs have this property with high probability [79]. As such weakly-Ramanujan graphs are also expander graphs by a straightforward extension of Lems. 20 and 21, this in principle displays a large class of potential power grid topologies that would be eligible for an exponential quantum speedup. However, due to the very high connectivity required in expander graphs (e.g., the diameter scaling merely logarithmically wrt. the number of nodes [80]), it is questionable if power grids can reasonably be structured accordingly in practice. Even if power grids could take the form of expanders, it is contestable if currently existing power grids could be adapted accordingly, or if this would only be a consideration for the architecture of newly assembled power grids. Nevertheless, some literature already exists that motivates a condition-number-minimizing design of power grids, see, e.g., Ref. [81].

B. Topology Optimization

Designing mechanical structures requires to find the optimal balance between functional factors like stiffness or aerodynamic properties and constraining factors such as cost, weight or space. Algorithmic approaches show potential in automatically exploring the solution space but are often limited by the costly evaluations of functional properties which requires complex numerical simulations or even experiments. Due to constraints in time and cost, only a few points in the design space can be evaluated and thus a global optimum is often not reachable. An improvement can either be obtained by speeding up the simulation and thus enabling more evaluations or finding a better optimization strategy that more efficiently explores the design space. While we focus on the former, the later will have to be target of investigation for future (numerical) experiments. A typical use case in the domain of topology optimization is finding the maximally stiff structure for a beam under a specific load and weight constraint (cf. [82, 83]). For simplicity, we limit the following description to a system comprised of only one single type of element organized in a uniform mesh. Note however, that such a discretization is often insufficient in problems of industrial relevance to yield accurate results for the simulated physical properties. Nevertheless, it is an important and meaningful step towards exploring real-world QuSO problems.

Definition 11 (Topology optimization by distribution of isotropic material). *By discretizing the domain $\Omega := [0, \omega_x] \times [0, \omega_y] \subset \mathbb{R}^2$ that shall contain the body of the mechanical structure into an $n_x \times n_y$ grid of uniform linear right-triangle-shaped finite elements as shown in Fig. 10, where $\omega_x, \omega_y, n_x, n_y \in \mathbb{N}$, a corresponding topology optimization problem can be mathematically described by*

$$\arg \min_{\substack{x \in X \subset \{0,1\}^{2n_x n_y} \\ \sum_i x_i / 2n_x n_y = v}} \bar{u}^\top K_x \bar{u}, \quad (11)$$

where the decision variables x denote whether the corresponding finite element with index i should be filled with material (i.e., $x_i = 1$) or not (i.e., $x_i = 0$), and $0 < v \leq 1$ is a given maximum fraction of volume to be filled with material. X denotes the set of physically realizable shapes, i.e., (1) each filled triangle is connected to another filled triangle by sharing two nodes, (2) the nodes on which external force is applied are part of a filled triangle and (3), the given fixed points are also part of a filled triangle. $(K_x)_{jk} := \sum_i (K_x^{(i)})_{\pi^{-1}(j,k)}$ denotes the entries of the global stiffness matrix which is assembled through the local stiffness matrices of each element $K_x^{(i)} := \Delta (B^{(i)})^\top D_x^{(i)} B^{(i)}$ and a projector π mapping the indices of the local degrees of freedom in the local stiffness matrices to the corresponding indices of the global degrees of freedom given some numbering of all nodes in the mesh. Here, $\Delta := \omega_x \omega_y / 2n_x n_y$ denotes the area of each finite element, and $B^{(i)}$ denotes the strain-

displacement matrix of the i -th finite element whose vertices $(x_1^{(i)}, y_1^{(i)}) \in \Omega$, $(x_2^{(i)}, y_2^{(i)}) \in \Omega$, and $(x_3^{(i)}, y_3^{(i)}) \in \Omega$ are enumerated counterclockwise, s.t.

$$B^{(i)} := \frac{1}{2\Delta} \begin{pmatrix} \beta_1^{(i)} & 0 & \beta_2^{(i)} & 0 & \beta_3^{(i)} & 0 \\ 0 & \gamma_1^{(i)} & 0 & \gamma_2^{(i)} & 0 & \gamma_3^{(i)} \\ \gamma_1^{(i)} & \beta_1^{(i)} & \gamma_2^{(i)} & \beta_2^{(i)} & \gamma_3^{(i)} & \beta_3^{(i)} \end{pmatrix}, \quad (12)$$

where $\beta_1^{(i)} := y_2^{(i)} - y_3^{(i)}$, $\beta_2^{(i)} := y_3^{(i)} - y_1^{(i)}$, $\beta_3^{(i)} := y_1^{(i)} - y_2^{(i)}$, $\gamma_1^{(i)} := x_3^{(i)} - x_2^{(i)}$, $\gamma_2^{(i)} := x_1^{(i)} - x_3^{(i)}$, and $\gamma_3^{(i)} := x_2^{(i)} - x_1^{(i)}$. Further, assuming all filled elements are made of identical isotropic material, the plane strain matrix $D_x^{(i)}$ is defined as

$$D_x^{(i)} := \frac{E(x_i)}{(1+\nu)(1-2\nu)} \begin{pmatrix} 1-\nu & \nu & 0 \\ \nu & 1-\nu & 0 \\ 0 & 0 & \frac{1-2\nu}{2} \end{pmatrix}, \quad (13)$$

where ν denotes the Poisson's ratio (e.g., $\nu = 0.3$ for typical structure steel), and $E(x_i) := E_{\min} + x_i (E_0 - E_{\min})$ the Young's modulus of each element, depending on whether it is filled (i.e., $E(x_i) = E_0$, where, e.g., $E_0 = 210000\text{MPa}$ for typical structure steel) or not (i.e., $E(x_i) = E_{\min} > 0$). Finally, \bar{u} denotes the vector of displacements for the degrees of freedom in the nodes of the structure of the finite element mesh, which is implicitly given through the system of equations $K_x \bar{u} = \bar{f}$, where \bar{f} is the vector of external forces acting on the structure for each degree of freedom. Note that due to the degrees of freedom in fixed nodes being fixed, we have to delete the rows and columns from K_x and \bar{u} that concern these degrees of freedom in all places where they appear in the definitions above (which we did not consider in this to enhance readability).

Remark 16 (Topology optimization is LinQuSO). Intuitively, the described optimization problem (cf. Ref. [84] for a similar formulation) describes the aim at finding a physically meaningful material assignment within a fixed volume fraction v that leads to minimal compliance $c(x) := \bar{u}^\top K_x \bar{u}$ of the structure under a given load \bar{f} . Even though further constraints and costs (e.g., ease of manufacturing, spatial constraints) could be included, we limit the discussion in this paper to only include the structure's compliance within the cost function as this already forms a LinQuSO problem, i.e., by defining $s(x) := K_x^+ \bar{f}$ and $u(s(x)) := s(x)^\top K_x s(x)$ it becomes clear, that the problem stated in Def. 11 is a LinQuSo problem (cf. Def. 4).

Remark 17 (Sparsity and condition number estimates). As the entries in the global stiffness matrix represent interactions of nodes in the mesh, the number of non-zero entries scales linearly with the maximum amount of neighbors any node can have. By employing the uniform mesh displayed in Fig. 10 with a horizontal and vertical degree of freedom for every node, K_x has a sparsity ≤ 26 ,

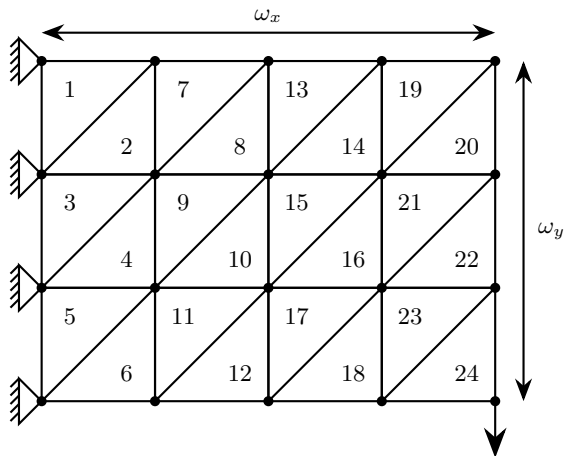


FIG. 10. Visualization of an example to the optimization problem defined in Def. 11, where $n_x = 4$, $n_y = 3$, and where the external force applied \vec{f} only acts upon the vertical degree of freedom of the bottom right node in the mesh. The numbers shown depict possible indices of the finite elements. The triangles to the left of the left-most grid nodes indicate that these nodes are fixed.

as every node's two degrees of freedom are affected by the degrees of freedom of its direct neighbours (there exist at maximum six neighbours with two DOFs in our mesh) and itself. Further, there exists an upper bound on the value of the maximum entry of each local stiffness matrix (due to such bounds being implied by definition for the strain-displacement matrix $B^{(i)}$ and the plane strain matrix $D_x^{(i)}$). Therefore, by the Gershgorin circle theorem Lem. 16, we can set a constant upper bound on the maximal singular value of the global stiffness matrix. For a lower bound on the smallest singular value of K_x , we resort to the well-known result of the condition number of the global stiffness matrix scaling as $\mathcal{O}(1/h^2)$, where h denotes the size of each finite element [85]. This implies that the condition number scales linearly in the dimension of the SLE $\mathcal{O}(N)$ and hence the smallest singular value correspondingly can be bound from below with a value $\mathcal{O}(1/N)$. Note however, that by switching from the here employed nodal basis of the finite element space to a hierarchical basis, the condition number could be reduced to $\mathcal{O}(\log N)$, enabling an exponential quantum speedup [85]. Future work will have to show if our approach can be generalized to the slightly altered decision-variable-dependent SLE that emerges from this different finite element space basis.

Having established the sparsity and bounds on the largest and smallest singular value, we now show how this problem can be solved with the framework of quantum algorithms proposed in Sec. III.

By representing the material assignments as a binary vector (where zero represents a void element and one a filled element), the conditional block encoding of K_x can be achieved with the complexity stated in Thm. 12 by

slightly adapting the quantum algorithm presented there to allow for the matrix entries of the type $c + x_k(a_{ij} - c)$ for $c := E_{\min}$ constant and a_{ij} denoting the entries of the global stiffness matrix K_x when $x_k = 1$ for all k . This adaption can be accomplished by analogously using Lem. 11 for block-encoding a matrix with entries a_{ij} while stopping before the AQE step to insert the UCU from Thm. 11 controlled on the matrix index registers to compute the value of the respective $x_{k(i,j)}$ on an ancillary qubit. Then we control the AQE on this ancilla to ensure that the value for a_{ij} is only respected if the corresponding $x_{k(i,j)}$ equals one, additionally we prepare an ancillary register to represent c in basis encoding and add an AQE of this register controlled on the respective decision variable $x_{k(i,j)}$ being zero. After that, we uncompute these steps (except for the AQE) and finally uncompute O_A to conclude the block-encoding. By applying the implementation setup from Fig. 8 for the UCU, we end up with an algorithm of complexity in the same order of magnitude as Thm. 12.

By using Thm. 13 with u_3 and Lem. 3 to input the external force vector \vec{f} we can implement QSim for the stated topology optimization problem. Finally to obtain a result for the topology optimization problem, we can run the QuSO solver defined in Thm. 10 by introducing respective penalty terms to ensure the physical meaningfulness of the result (i.e., $x \in X$).

V. DISCUSSION

In this article, we proposed a novel class of optimization problems, that require summary statistic information on the result of a simulation to compute the cost function or ensure the validity of constraints called Quantum Simulation-based Optimization (QuSO). Further, we introduced an efficient quantum algorithm to perform a specific type of digital to analog conversion to facilitate the combination of the QAOA and the QSVT to efficiently solve QuSO problems. Finally, we exemplified the application of the developed approach to achieve up to exponential quantum speedups for two use cases with potential practical relevance. More precisely, the simulation component of the QuSO problem can be solved in time $\tilde{\mathcal{O}}(\text{polylog}(N)\kappa^*s)$ compared to the conjugate gradient method's (i.e., the classical state of the art) $\mathcal{O}(N\kappa s)$ for indefinite $N \times N$ matrices (and $\mathcal{O}(N\kappa s)$ for positive definite matrices) with an upper bound on the condition number $\kappa^* \geq \kappa$ and sparsity s . In practice, the potential quantum speedup is thus quadratic for condition numbers that scale linearly with the size of the system (e.g., in practical instances for the optimal power flow problem) and exponential if the condition number scales at most logarithmically with the dimension of the SLE (e.g., for the optimal power flow problem on expander graphs). As almost all subroutines used in our quantum solver for QuSO problems require a substantial amount of error-corrected quantum hardware, the first

examples for practically relevant quantum speedup will likely require a very small condition number (cf. [86]). While practically relevant use cases with constant or at most logarithmic condition number exist [85, 87–91], their practical problem instances can often already be solved within reasonable computational costs using classical algorithms, as these are already quasi-linear in the dimension of the SLE. Therefore, the quadratic quantum speedup to be gained for problems with linear condition number might even have a bigger effect in practice, when quasi-constant-overhead quantum error correction [92] is available in practice.

Once sufficiently large quantum hardware is available to solve real world instances of QuSO problems, the performance of the QAOA against classically employed simulation-based optimization algorithms like Monte-Carlo search, genetic algorithms, response surface methodology, or the SIMP method for topology optimization, should be benchmarked to evaluate if our QuSO solver can also provide practical wallclock-time speedups or even a better solution quality. Based on the fact that typical state-of-the-art optimization algorithms like branch and bound are not necessarily well-suited to solve optimization problems with very large systems of linear equations as constraints, such a benchmark will be particularly interesting, as BnB solvers are typically the state of the art for practically all combinatorial optimization problems that were predominantly the topic of past quantum optimization benchmarks. Another potentially relevant difference to classical state-of-the-art simulation-based optimization solvers, is that our QAOA-driven approach does not necessarily need multiple iterations to find optimal solutions, i.e., measurements from a single quantum circuit can already suffice (assuming predefined or pretrained QAOA parameters, cf. [45]).

The provided examples demonstrate the ability of the proposed framework of quantum subroutines to solve practically relevant QuSO problems. Stemming on theoretical results from spectral graph theory as well as mesh structure in the finite element method, we exemplified the process of computing the required bounds for the largest and smallest singular values as well as an upper bound on the sparsity. The employed approach for the optimal power flow simulation in context of the unit commitment problem shows the first practically relevant quantum algorithm in the context of recent research in this domain by effectively bypassing the output problem [71, 93–98]. A logical next step for exploring the applicability of quantum simulation speedups in this context would be investigating the non-linear form of the power flow equations – cf. Refs. [99, 100] for respective classical (but also typically highly approximative) approaches. For the topology optimization use case, we showed a quadratic speedup analogous to the power flow simulation (where speedup is only of order $\mathcal{O}(n^{3/2})$). Further research has to show if our framework of quantum algorithmic subroutines can be applied, or sufficiently extended, to allow for an exponential speedup either using

suitable preconditioners [101–103] or, e.g., a hierarchical basis for the mesh [85]. Notably, the exploration of preconditioners might be especially interesting, as recent literature showed efficient implementations for the respective block-encoding [104]. In general, we strongly expect the existence of more efficient approaches to conduct the block-encoding for simple FEM models, as the matrix entries can easily be described by simple algebraic functions. This could open up QuSO use cases that do not suffer from linear or even quadratic space requirements for the data input, but rather operate within logarithmic space requirements, which would allow for significantly sooner practical applications of the presented approach.

Future work may focus on the identification of other practically relevant QuSO problems. Central questions to decide the applicability of the presented framework are the sparsity of the SLE, bounds on the smallest non-zero and the largest singular values, and optionally any mathematically exploitable structure in A_x and \tilde{b}_x for corresponding state preparation oracles. Beyond this, non-linear as well as quantum-native use cases should be investigated accordingly.

ACKNOWLEDGMENTS

This paper was partially funded by the German Federal Ministry for Economic Affairs and Climate Action through the funding program “Quantum Computing – Applications for the industry” based on the allowance

“Development of digital technologies” (contract number: 01MQ22008A). PA acknowledges support from the Munich Quantum Valley, which is supported by the Bavarian state government with funds from the Hightech Agenda Bayern Plus.

-
- [1] R. P. Feynman, Simulating physics with computers, *Int. J. Theor. Phys.* **21**, 467–488 (1982).
- [2] S. Lloyd, Universal quantum simulators, *Science* **273**, 1073–1078 (1996).
- [3] A. W. Harrow, A. Hassidim, and S. Lloyd, Quantum algorithm for linear systems of equations, *Phys. Rev. Lett.* **103**, 150502 (2009).
- [4] A. Ambainis, Variable time amplitude amplification and quantum algorithms for linear algebra problems, in *29th International Symposium on Theoretical Aspects of Computer Science (STACS 2012)*, Leibniz International Proceedings in Informatics (LIPIcs), Vol. 14, edited by C. Dürr and T. Wilke (Schloss Dagstuhl – Leibniz-Zentrum für Informatik, Dagstuhl, Germany, 2012) pp. 636–647.
- [5] D. W. Berry, A. M. Childs, and R. Kothari, Hamiltonian simulation with nearly optimal dependence on all parameters, in *2015 IEEE 56th Annual Symposium on Foundations of Computer Science* (2015) pp. 792–809.
- [6] A. M. Childs, R. Kothari, and R. D. Somma, Quantum algorithm for systems of linear equations with exponentially improved dependence on precision, *SIAM Journal on Computing* **46**, 1920–1950 (2017).
- [7] A. Gilyén, Y. Su, G. H. Low, and N. Wiebe, Quantum singular value transformation and beyond: exponential improvements for quantum matrix arithmetics (2018), [arXiv:1806.01838 \[quant-ph\]](https://arxiv.org/abs/1806.01838).
- [8] Y. Subaşı, R. D. Somma, and D. Orsucci, Quantum algorithms for systems of linear equations inspired by adiabatic quantum computing, *Phys. Rev. Lett.* **122**, 060504 (2019).
- [9] L. Lin and Y. Tong, Optimal polynomial based quantum eigenstate filtering with application to solving quantum linear systems, *Quantum* **4**, 361 (2020).
- [10] D. Orsucci and V. Dunjko, On solving classes of positive-definite quantum linear systems with quadratically improved runtime in the condition number, *Quantum* **5**, 573 (2021).
- [11] Y. Cao, A. Papageorgiou, I. Petras, J. Traub, and S. Kais, Quantum algorithm and circuit design solving the poisson equation, *New Journal of Physics* **15**, 013021 (2013).
- [12] P. C. S. Costa, S. Jordan, and A. Ostrander, Quantum algorithm for simulating the wave equation, *Phys. Rev. A* **99**, 012323 (2019).
- [13] N. Linden, A. Montanaro, and C. Shao, Quantum vs. Classical Algorithms for Solving the Heat Equation, *Commun. Math. Phys.* **395**, 601–641 (2022).
- [14] R. Babbush, D. W. Berry, R. Kothari, R. D. Somma, and N. Wiebe, Exponential quantum speedup in simulating coupled classical oscillators, *Phys. Rev. X* **13**, 041041 (2023).
- [15] A. M. Childs, J.-P. Liu, and A. Ostrander, High-precision quantum algorithms for partial differential equations, *Quantum* **5**, 574 (2021).
- [16] S. Jin, N. Liu, and Y. Yu, Quantum simulation of partial differential equations via schrodingerisation (2022), [arXiv:2212.13969 \[quant-ph\]](https://arxiv.org/abs/2212.13969).
- [17] S. K. Leyton and T. J. Osborne, A quantum algorithm to solve nonlinear differential equations (2008), [arXiv:0812.4423 \[quant-ph\]](https://arxiv.org/abs/0812.4423).
- [18] S. Lloyd, G. D. Palma, C. Gokler, B. Kiani, Z.-W. Liu, M. Marvian, F. Tennie, and T. Palmer, Quantum algorithm for nonlinear differential equations (2020), [arXiv:2011.06571 \[quant-ph\]](https://arxiv.org/abs/2011.06571).
- [19] J.-P. Liu, H. Øie Kolden, H. K. Krovi, N. F. Loureiro, K. Trivisa, and A. M. Childs, Efficient quantum algorithm for dissipative nonlinear differential equations, *Proceedings of the National Academy of Sciences* **118**, e2026805118 (2021).
- [20] I. Joseph, Koopman–von neumann approach to quantum simulation of nonlinear classical dynamics, *Phys. Rev. Res.* **2**, 043102 (2020).
- [21] I. Y. Dodin and E. A. Startsev, On applications of quantum computing to plasma simulations, *Physics of Plasmas* **28**, 092101 (2021).
- [22] S. Jin and N. Liu, Quantum algorithms for nonlinear partial differential equations, *Bulletin des Sciences Mathématiques* **194**, 103457 (2024).
- [23] I. Kerenidis and A. Prakash, Quantum Recommendation Systems, in *8th Innovations in Theoretical Computer Science Conference (ITCS 2017)*, Leibniz International Proceedings in Informatics (LIPIcs), Vol. 67, edited by C. H. Papadimitriou (Schloss Dagstuhl – Leibniz-Zentrum für Informatik, Dagstuhl, Germany, 2017) pp. 49:1–49:21.
- [24] N. Guseynov, X. Huang, and N. Liu, Explicit gate construction of block-encoding for hamiltonians needed for simulating partial differential equations (2024), [arXiv:2405.12855 \[quant-ph\]](https://arxiv.org/abs/2405.12855).
- [25] D. Camps, L. Lin, R. Van Beeumen, and C. Yang, Explicit quantum circuits for block encodings of certain sparse matrices, *SIAM Journal on Matrix Analysis and Applications* **45**, 801–827 (2024).
- [26] X. Sun, G. Tian, S. Yang, P. Yuan, and S. Zhang, Asymptotically optimal circuit depth for quantum state preparation and general unitary synthesis, *IEEE Transactions on Computer-Aided Design of Integrated Circuits and Systems* **42**, 3301–3314 (2023).
- [27] P. Yuan and S. Zhang, Optimal (controlled) quantum state preparation and improved unitary synthesis by quantum circuits with any number of ancillary qubits, *Quantum* **7**, 956 (2023).
- [28] M. Paris and J. Rehacek, *Quantum state estimation*, Vol. 649 (Springer Science & Business Media, 2004).
- [29] A. Gosavi, *Simulation-Based Optimization: Parametric*

- Optimization Techniques and Reinforcement Learning*, 2nd ed. (Springer New York, NY, 2015).
- [30] S. Amaran, N. V. Sahinidis, B. Sharda, and S. J. Bury, Simulation optimization: a review of algorithms and applications, *4OR* **12**, 301–333 (2014).
- [31] W. Trigueiro de Sousa Junior, J. A. Barra Montevechi, R. de Carvalho Miranda, and A. Teberga Campos, Discrete simulation-based optimization methods for industrial engineering problems: A systematic literature review, *Computers & Industrial Engineering* **128**, 526–540 (2019).
- [32] E. Tekin and I. Sabuncuoglu, Simulation optimization: A comprehensive review on theory and applications, *IIE Transactions* **36**, 1067–1081 (2004).
- [33] L.-F. Wang and L.-Y. Shi, Simulation optimization: A review on theory and applications, *Acta Automatica Sinica* **39**, 1957–1968 (2013).
- [34] R. H. Myers, D. C. Montgomery, and C. M. Anderson-Cook, *Response surface methodology: process and product optimization using designed experiments* (John Wiley & Sons, 2016).
- [35] V. O. Balabanov and R. T. Haftka, Topology optimization of transport wing internal structure, *Journal of aircraft* **33**, 232–233 (1996).
- [36] Y. Carson and A. Maria, Simulation optimization: Methods and applications, in *Winter Simulation Conference Proceedings*, (1997) pp. 118–126.
- [37] J. April, F. Glover, J. P. Kelly, and M. Laguna, Practical introduction to simulation optimization, in *Proceedings of the 2003 Winter Simulation Conference, 2003.*, Vol. 1 (2003) pp. 71–78.
- [38] F. Gaitan, Finding flows of a Navier–Stokes fluid through quantum computing, *npj Quantum Inf.* **6**, 61 (2020).
- [39] E. Farhi, J. Goldstone, S. Gutmann, and M. Sipser, Quantum computation by adiabatic evolution (2000), [arXiv:quant-ph/0001106](https://arxiv.org/abs/quant-ph/0001106) [quant-ph].
- [40] M. Born and V. Fock, Beweis des Adiabatsatzes, *Zeitschrift für Phys.* **51**, 165–180 (1928).
- [41] A. Lucas, Ising formulations of many np problems, *Frontiers in Physics* **2**, 74887 (2014).
- [42] D. Herman, R. Shaydulin, Y. Sun, S. Chakrabarti, S. Hu, P. Minssen, A. Rattew, R. Yalovetzky, and M. Pistoia, Constrained optimization via quantum Zeno dynamics, *Commun. Phys.* **6**, 219 (2023).
- [43] E. Farhi, J. Goldstone, and S. Gutmann, A quantum approximate optimization algorithm (2014), [arXiv:1411.4028](https://arxiv.org/abs/1411.4028) [quant-ph].
- [44] K. Tamura, T. Shirai, H. Katsura, S. Tanaka, and N. Togawa, Performance comparison of typical binary-integer encodings in an ising machine, *IEEE Access* **9**, 81032–81039 (2021).
- [45] S. H. Sack and M. Serbyn, Quantum annealing initialization of the quantum approximate optimization algorithm, *Quantum* **5**, 491 (2021).
- [46] K. Mitarai, M. Negoro, M. Kitagawa, and K. Fujii, Quantum circuit learning, *Phys. Rev. A* **98**, 032309 (2018).
- [47] A. Bärttschi and S. Eidenbenz, Grover mixers for qaoa: Shifting complexity from mixer design to state preparation, in *2020 IEEE International Conference on Quantum Computing and Engineering (QCE)* (2020) pp. 72–82.
- [48] T. Häner, M. Roetteler, and K. M. Svore, Optimizing quantum circuits for arithmetic (2018), [arXiv:1805.12445](https://arxiv.org/abs/1805.12445) [quant-ph].
- [49] P. Stougiannidis, J. Stein, D. Bucher, S. Zielinski, C. Linnhoff-Popien, and S. Feld, Approximative lookup-tables and arbitrary function rotations for facilitating NISQ-implementations of the HHL and beyond, in *2023 IEEE International Conference on Quantum Computing and Engineering (QCE)*, Vol. 01 (2023) pp. 151–160.
- [50] A. Shukla and P. Vedula, An efficient quantum algorithm for preparation of uniform quantum superposition states, *Quantum Inf. Process.* **23**, 38 (2024).
- [51] I. Kerenidis and A. Prakash, Quantum Recommendation Systems, in *8th Innovations in Theoretical Computer Science Conference (ITCS 2017)*, Leibniz International Proceedings in Informatics (LIPIcs), Vol. 67, edited by C. H. Papadimitriou (Schloss Dagstuhl – Leibniz-Zentrum für Informatik, Dagstuhl, Germany, 2017) pp. 49:1–49:21.
- [52] L. Wossnig, Z. Zhao, and A. Prakash, Quantum linear system algorithm for dense matrices, *Phys. Rev. Lett.* **120**, 050502 (2018).
- [53] C. Wang and L. Wossnig, A quantum algorithm for simulating non-sparse hamiltonians, *Quantum Information and Computation* **20**, 597–615 (2020).
- [54] G. H. Low, T. J. Yoder, and I. L. Chuang, Methodology of resonant equiangular composite quantum gates, *Phys. Rev. X* **6**, 041067 (2016).
- [55] G. H. Low and I. L. Chuang, Optimal hamiltonian simulation by quantum signal processing, *Phys. Rev. Lett.* **118**, 010501 (2017).
- [56] Y. Dong, L. Lin, H. Ni, and J. Wang, Robust iterative method for symmetric quantum signal processing in all parameter regimes (2023), [arXiv:2307.12468](https://arxiv.org/abs/2307.12468) [quant-ph].
- [57] D. Motlagh and N. Wiebe, Generalized quantum signal processing (2024), [arXiv:2308.01501](https://arxiv.org/abs/2308.01501) [quant-ph].
- [58] C. Sünderhauf, Generalized quantum singular value transformation (2023), [arXiv:2312.00723](https://arxiv.org/abs/2312.00723) [quant-ph].
- [59] J. M. Martyn, Z. M. Rossi, A. K. Tan, and I. L. Chuang, Grand unification of quantum algorithms, *PRX Quantum* **2**, 040203 (2021).
- [60] Y. Dong, X. Meng, K. B. Whaley, and L. Lin, Efficient phase-factor evaluation in quantum signal processing, *Phys. Rev. A* **103**, 042419 (2021).
- [61] L. Lin, *Lecture notes on quantum algorithms for scientific computation* (2022), [arXiv:2201.08309](https://arxiv.org/abs/2201.08309) [quant-ph].
- [62] A. G. Rattew and P. Rebentrost, Non-linear transformations of quantum amplitudes: Exponential improvement, generalization, and applications (2023), [arXiv:2309.09839](https://arxiv.org/abs/2309.09839) [quant-ph].
- [63] A. Y. Kitaev, Quantum measurements and the abelian stabilizer problem (1995), [arXiv:quant-ph/9511026](https://arxiv.org/abs/quant-ph/9511026) [quant-ph].
- [64] R. Cleve, A. Ekert, C. Macchiavello, and M. Mosca, Quantum amplitude amplification and estimation, *Proc. R. Soc. Lond. A.* **454**, 339–354 (1998).
- [65] G. Brassard, M. Mosca, and A. Tapp, Quantum amplitude amplification and estimation, *Contemporary Mathematics* **305**, 53–74 (2002).
- [66] Y. Liao, M.-H. Hsieh, and C. Ferrie, Quantum optimization for training quantum neural networks (2021), [arXiv:2103.17047](https://arxiv.org/abs/2103.17047) [quant-ph].
- [67] M. H. Stone, Applications of the theory of boolean rings to general topology, *Transactions of the American Mathematical Society* **41**, 375–481 (1937).

- [68] J. Stein, F. Chamanian, M. Zorn, J. Nüblein, S. Zielinski, M. Kölle, and C. Linnhoff-Popien, Evidence that puho outperforms qubo when solving continuous optimization problems with the qaoa, in *Proceedings of the Companion Conference on Genetic and Evolutionary Computation*, GECCO '23 Companion (Association for Computing Machinery, New York, NY, USA, 2023) p. 2254–2262.
- [69] H. M. Trent, A note on the enumeration and listing of all possible trees in a connected linear graph, *Proceedings of the National Academy of Sciences* **40**, 1004–1007 (1954).
- [70] G. R. Kirchhoff, On the solution of the equations obtained from the investigation of the linear distribution of galvanic currents, *IRE Transactions on Circuit Theory* **5**, 4–7 (1958).
- [71] P. Pareek, A. Jayakumar, C. Coffrin, and S. Misra, Demystifying quantum power flow: Unveiling the limits of practical quantum advantage (2024), arXiv:2402.08617 [quant-ph].
- [72] M. Chethan and R. Kuppan, A review of FACTS device implementation in power systems using optimization techniques, *J. Eng. Appl. Sci.* **71**, 18 (2024).
- [73] B. Mohar, Eigenvalues, diameter, and mean distance in graphs, *Graphs Comb.* **7**, 53–64 (1991).
- [74] S. A. Gershgorin, Über die Abgrenzung der Eigenwerte einer Matrix., *Bull. Acad. Sci. URSS* **1931**, 749–754 (1931).
- [75] A.-L. Cauchy, Sur l'équation à l'aide de laquelle on détermine les inégalités séculaires des mouvements des planètes, in *Euvres complètes (Iieme Série)*, Cambridge Library Collection – Mathematics, Vol. 9 (Gauthier-Villars, 1829) p. 174–195.
- [76] J. Cheeger, A lower bound for the smallest eigenvalue of the laplacian, in *Problems in Analysis*, edited by R. C. Gunning (Princeton University Press, Princeton, 1971) pp. 195–200.
- [77] A.-L. Cauchy, *Exercices de mathématiques* (De Bure Frères, 1829).
- [78] M. Morgenstern, Existence and explicit constructions of $q + 1$ regular ramanujan graphs for every prime power q , *Journal of Combinatorial Theory, Series B* **62**, 44–62 (1994).
- [79] J. Friedman, A proof of alon's second eigenvalue conjecture, in *Proceedings of the Thirty-Fifth Annual ACM Symposium on Theory of Computing*, STOC '03 (Association for Computing Machinery, New York, NY, USA, 2003) p. 720–724.
- [80] F. R. K. Chung, Diameters and eigenvalues, *Journal of the American Mathematical Society* **2**, 187–196 (1989).
- [81] F. B. Thiam and C. L. DeMarco, Optimal transmission expansion via intrinsic properties of power flow conditioning, in *North American Power Symposium 2010* (2010) pp. 1–8.
- [82] M. P. Bendsoe and O. Sigmund, *Topology optimization: theory, methods, and applications* (Springer Science & Business Media, 2013).
- [83] O. C. Zienkiewicz, R. L. Taylor, and J. Z. Zhu, *The finite element method: its basis and fundamentals*, 5th ed., Vol. 1 (Butterworth-Heinemann, 2000).
- [84] E. Andreassen, A. Clausen, M. Schevenels, B. S. Lazarov, and O. Sigmund, Efficient topology optimization in MATLAB using 88 lines of code, *Struct. Multi-discip. Optim.* **43**, 1–16 (2011).
- [85] H. Yserentant, On the multi-level splitting of finite element spaces, *Numer. Math.* **49**, 379–412 (1986).
- [86] R. Babbush, J. R. McClean, M. Newman, C. Gidney, S. Boixo, and H. Neven, Focus beyond quadratic speedups for error-corrected quantum advantage, *PRX Quantum* **2**, 010103 (2021).
- [87] R. E. Bank, T. F. Dupont, and H. Yserentant, The hierarchical basis multigrid method, *Numer. Math.* **52**, 427–458 (1988).
- [88] R. E. Bank and L. R. Scott, On the conditioning of finite element equations with highly refined meshes, *SIAM Journal on Numerical Analysis* **26**, 1383–1394 (1989).
- [89] J. H. Bramble, J. E. Pasciak, J. P. Wang, and J. Xu, Convergence estimates for product iterative methods with applications to domain decomposition, *Mathematics of Computation* **57**, 1–21 (1991).
- [90] H. Yserentant, Old and new convergence proofs for multigrid methods, *Acta Numerica* **2**, 285–326 (1993).
- [91] M. Adams, Evaluation of three unstructured multigrid methods on 3d finite element problems in solid mechanics, *International Journal for Numerical Methods in Engineering* **55**, 519–534 (2002).
- [92] O. Fawzi, A. Grospellier, and A. Leverrier, Constant overhead quantum fault-tolerance with quantum expander codes, in *2018 IEEE 59th Annual Symposium on Foundations of Computer Science (FOCS)* (2018) pp. 743–754.
- [93] F. Feng, Y. Zhou, and P. Zhang, Quantum power flow, *IEEE Transactions on Power Systems* **36**, 3810–3812 (2021).
- [94] F. Gao, G. Wu, S. Guo, W. Dai, and F. Shuang, Solving dc power flow problems using quantum and hybrid algorithms, *Applied Soft Computing* **137**, 110147 (2023).
- [95] F. Amani, R. Mahroo, and A. Kargarian, Quantum-enhanced dc optimal power flow, in *2023 IEEE Texas Power and Energy Conference (TPEC)* (2023) pp. 1–6.
- [96] B. Sævarsson, S. Chatzivasileiadis, H. Jóhannsson, and J. Østergaard, Quantum computing for power flow algorithms: Testing on real quantum computers, in *Proceedings of 11th Bulk Power Systems Dynamics and Control Symposium (IREP 2022)* (2024) <https://arxiv.org/abs/2204.14028>.
- [97] D. Neufeld, S. Fathi Hafshejani, D. Gaur, and R. Benkoczi, A hybrid quantum algorithm for load flow, in *Power, Energy and Electrical Engineering* (IOS Press, 2024) pp. 589–600.
- [98] J. Liu, H. Zheng, M. Hanada, K. Setia, and D. Wu, Quantum power flows: from theory to practice, *Quantum Mach. Intell.* **6**, 55 (2024).
- [99] L. L. Freris and A. M. Sasson, Investigation of the load-flow problem, in *Proceedings of the institution of electrical engineers*, Vol. 115 (IET, 1968) pp. 1459–1470.
- [100] S. Tripathy, G. D. Prasad, O. Malik, and G. Hope, Load-flow solutions for ill-conditioned power systems by a newton-like method, *IEEE Transactions on Power Apparatus and Systems* **PAS-101**, 3648–3657 (1982).
- [101] J. H. Bramble, J. E. Pasciak, and J. Xu, Parallel multi-level preconditioners, *Mathematics of computation* **55**, 1–22 (1990).
- [102] F. A. Bornemann, *A Sharpened Condition Number Estimate for the BPX Preconditioner of Elliptic Finite Element Problems on Highly Nonuniform Triangulations.*, Tech. Rep. SC-91-09 (ZIB, Takustr. 7, 14195 Berlin,

1991).

- [103] J. Maes and A. Bultheel, A hierarchical basis preconditioner for the biharmonic equation on the sphere, *IMA Journal of Numerical Analysis* **26**, 563–583 (2006).
- [104] M. Deiml and D. Peterseim, *Quantum realization of the finite element method* (2024), arXiv:2403.19512 [quant-ph].
- [105] J. P. G. L. Dirichlet, Sur la convergence des séries trigonométriques qui servent à représenter une fonction arbitraire entre des limites données., *Journal für die reine und angewandte Mathematik* **4**, 157–169 (1829).

Appendix A: Complexities of subroutines

The complexities of all algorithms employed for data input, processing and output are displayed in Table I.

Appendix B: Implementations of the diagonal block-encoding operators G_p and W_p

The operators G_p and W_p as defined in Ref. [62] are displayed in Fig. 11 and Fig. 12.

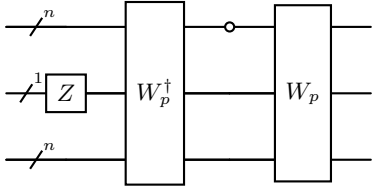


FIG. 11. Quantum circuit implementing the operator G_p as used in the implementation of Thm. 6.

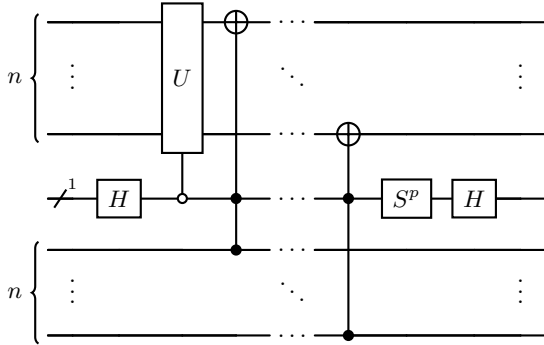


FIG. 12. Quantum circuit implementing the operator W_p as used in the implementation of Thm. 6.

Appendix C: Polynomial Approximation of the absolute value function

In the following, we provide a proof for Lem. 13, i.e., show that the polynomial stated in Lem. 13 provides an

efficient and accurate approximation of the absolute value function $|\cdot| : [-1, 1] \rightarrow [-1, 1]$.

Definition 12 (Fourier series). *The Fourier series of any 2π -periodic function $f \in L^1([0, 2\pi])$ is defined as*

$$(\mathcal{F}f)(x) := \frac{a_0}{2} + \sum_{k=1}^{\infty} (a_k \cos kx + b_k \sin kx) \quad (\text{C1})$$

via the Fourier coefficients $a_k := \frac{1}{\pi} \int_0^{2\pi} f(x) \cos kx dx$ and $b_k := \frac{1}{\pi} \int_0^{2\pi} f(x) \sin kx dx$ for $k \in \mathbb{N}$ and $a_0 := \frac{1}{\pi} \int_0^{2\pi} f(x) dx$.

Lemma 22. *The Fourier series of $f(x) := |\cos(x)|$ for $x \in \mathbb{R}$ is given by*

$$(\mathcal{F}f)(x) = \frac{2}{\pi} + \frac{4}{\pi} \sum_{k=1}^{\infty} \frac{(-1)^{k+1}}{4k^2 - 1} \cos(2kx) \quad (\text{C2})$$

Proof. As $f(x) = |\cos(x)|$ is a 2π -periodic function in $L^1([0, 2\pi])$, the Fourier coefficients a_k and b_k for $k \in \mathbb{N}$ can be determined according to the definition stated in Def. 12. For the a_k coefficients we thus get

$$\begin{aligned} a_k &= \frac{1}{\pi} \int_0^{2\pi} f(x) \cos(kx) dx \\ &= \frac{1}{\pi} \int_0^{2\pi} |\cos(x)| \cos(kx) dx \\ &= \frac{2}{\pi} \left(\underbrace{\int_0^{\frac{\pi}{2}} \cos(x) \cos(kx) dx}_{I_1 :=} - \underbrace{\int_{\frac{\pi}{2}}^{\pi} \cos(x) \cos(kx) dx}_{I_2 :=} \right) \end{aligned}$$

Using the trigonometric identity $\cos(x) \cos(kx) = \frac{1}{2} (\cos((k+1)x) + \cos((k-1)x))$, we can compute I_1 as

$$I_1 = \frac{1}{2} \left(\underbrace{\int_0^{\frac{\pi}{2}} \cos((k+1)x) dx}_{I_{11} :=} + \underbrace{\int_0^{\frac{\pi}{2}} \cos((k-1)x) dx}_{I_{12} :=} \right)$$

By substituting $u := (k+1)x$ in I_{11} , we get

$$\begin{aligned} I_{11} &= \int_0^{\frac{\pi}{2}} \cos(u) \frac{du}{k+1} = \frac{1}{k+1} \int_0^{\frac{\pi}{2}} \cos(u) du \\ &= \frac{1}{k+1} \sin\left(\left(k+1\right)\frac{\pi}{2}\right). \end{aligned}$$

Analogously substituting $v := (k-1)x$ in I_{12} yields

$$\begin{aligned} I_{12} &= \int_0^{\frac{\pi}{2}} \cos(v) \frac{dv}{k-1} = \frac{1}{k-1} \int_0^{\frac{\pi}{2}} \cos(v) dv \\ &= \frac{1}{k-1} \sin\left(\left(k-1\right)\frac{\pi}{2}\right). \end{aligned}$$

Combining these results, I_1 takes the form of

$$\begin{aligned} I_1 &= \frac{1}{2} (I_{11} + I_{12}) \\ &= \frac{1}{2} \left(\frac{1}{k+1} \sin\left(\left(k+1\right)\frac{\pi}{2}\right) + \frac{1}{k-1} \sin\left(\left(k-1\right)\frac{\pi}{2}\right) \right). \end{aligned}$$

Data Input				
operation	qAlgo	depth + query complexity	space	#ancillas
$\mathbb{R}^N \rightarrow \mathcal{H}^{\otimes n}$ $b \mapsto b\rangle$	QStPr (Lem. 3)	$\mathcal{O}(\log(N)) + 0$	$\mathcal{O}(\log N)$	$\mathcal{O}(N)$
$\mathbb{R}^N \rightarrow \mathcal{H}^{\otimes n}$ $b_x \mapsto b_x\rangle$	QStPr (Lem. 9)	$\mathcal{O}(\log(N)) + 0$	$\mathcal{O}(\log N)$	$\mathcal{O}(N^2)$
$\mathbb{R}^{N \times N} \rightarrow \text{SU}(n)$ $A \mapsto U_A$	OBE (Lem. 11)	$\tilde{\mathcal{O}}(\log(n)) + \mathcal{O}(\log(N))$	$\mathcal{O}(n + 3)$	$\mathcal{O}(N + \log 1/\varepsilon)$
$\mathbb{R}^{N \times N} \rightarrow \text{SU}(n)$ $A_x \mapsto U_{A_x}$	OBE (Lem. 12)	$\tilde{\mathcal{O}}(\log(n)) + \mathcal{O}(\log(N))$	$\mathcal{O}(n + 3)$	$\mathcal{O}(N^2 + \log 1/\varepsilon)$
Data Processing				
$\text{SU}(n) \rightarrow \text{SU}(n)$ $U_A \mapsto U_{A^+}$	QSVT (Thm. 5)	$\mathcal{O}(1) + \mathcal{O}(\kappa \log(\frac{\kappa}{\varepsilon}))$	$\mathcal{O}(\log N)$	$\mathcal{O}(1)$
$\text{SU}(n) \rightarrow \text{SU}(n)$ $U_\psi \mapsto U_{ \psi\rangle}$	QSVT (Lem. 13)	$\mathcal{O}(n/\varepsilon) + \mathcal{O}(1/\varepsilon)$	$\mathcal{O}(n)$	$\mathcal{O}(1/\varepsilon)$
Extracting Summary Statistic Information				
$\text{SU}(n) \rightarrow [-0.5, 0.5]$ $U_\psi \mapsto \psi_i\rangle$	QAE (Thm. 9)	$\mathcal{O}(1/\varepsilon\delta) + \mathcal{O}(1/\varepsilon\delta)$	$\mathcal{O}(n + \log 1/\varepsilon\delta)$	$\mathcal{O}(1)$
$\text{SU}(n) \times \text{SU}(n) \rightarrow [0, 1]$ $U_\varphi, U_\psi \mapsto \langle \varphi \psi \rangle $	QAE (Cor. 3)	$\mathcal{O}(1/\varepsilon\delta) + \mathcal{O}(1/\varepsilon\delta)$	$\mathcal{O}(n + \log 1/\varepsilon\delta)$	$\mathcal{O}(1)$
$\text{SU}(n) \times \text{SU}(n) \rightarrow [-1, 1]$ $U_H, U_\psi \mapsto \langle \psi H \psi \rangle$	QAE (Lem. 7)	$\mathcal{O}(1/\varepsilon\delta) + \mathcal{O}(1/\varepsilon\delta)$	$\mathcal{O}(n + \log 1/\varepsilon\delta)$	$\mathcal{O}(1)$

TABLE I. Quantum basic linear algebra subroutines (qBLAS) used in this article and their complexities. We use the definition $N := 2^n$, where $n \in \mathbb{N}$ and assume that all vectors are normalized and all matrices are real and have a spectral norm lesser or equal than 1.

As I_2 is equivalent to I_1 up to the integration interval, we get

$$\begin{aligned}
I_2 &= \frac{1}{2} \left(\int_{\frac{\pi}{2}}^{\pi} \cos(kx + x) dx + \int_{\frac{\pi}{2}}^{\pi} \cos(kx - x) dx \right) \\
&= \frac{1}{2} \left(\frac{1}{k+1} (\sin((k+1)\pi) - \sin((k+1)\frac{\pi}{2})) \right) \\
&\quad + \frac{1}{2} \left(\frac{1}{k-1} (\sin((k-1)\pi) - \sin((k-1)\frac{\pi}{2})) \right).
\end{aligned}$$

Therefore we can now simplify a_k into

$$\begin{aligned}
a_k &= \frac{2}{\pi} (I_1 - I_2) \\
&= \frac{1}{\pi} \left(\frac{2 \sin((k+1)\frac{\pi}{2})}{k+1} + \frac{2 \sin((k-1)\frac{\pi}{2})}{k-1} \right) \\
&= \frac{2}{\pi} \left(\frac{\sin((k+1)\frac{\pi}{2})}{k+1} + \frac{\sin((k-1)\frac{\pi}{2})}{k-1} \right).
\end{aligned}$$

Further, we recognize that for any odd k , i.e., $k = 2m + 1$ with $m \in \mathbb{N}$, we have

$$\begin{aligned}
&\frac{\sin((2m+1+1)\frac{\pi}{2})}{2m+1+1} + \frac{\sin((2m+1-1)\frac{\pi}{2})}{2m+1-1} \\
&= \frac{\sin((2(m+1))\frac{\pi}{2})}{2(m+1)} + \frac{\sin((2m)\frac{\pi}{2})}{2m} = 0,
\end{aligned}$$

such that we only need to consider even k , allowing for the substitution $k \mapsto 2k$ and yielding

$$\begin{aligned}
a_k &= \frac{2}{\pi} \left(\frac{\sin((2k+1)\frac{\pi}{2})}{2k+1} + \frac{\sin((2k-1)\frac{\pi}{2})}{2k-1} \right) \\
&= \frac{2}{\pi} \left(\frac{(-1)^k}{2k+1} + \frac{-(-1)^k}{2k-1} \right) \\
&= \frac{2(-1)^k}{\pi} \left(\frac{1}{2k+1} - \frac{1}{2k-1} \right) \\
&= \frac{2(-1)^k}{\pi} \left(\frac{(2k-1) - (2k+1)}{(2k+1)(2k-1)} \right) \\
&= \frac{2(-1)^k}{\pi} \cdot \frac{-2}{(2k+1)(2k-1)} \\
&= \frac{4(-1)^{k+1}}{\pi} \cdot \frac{1}{4k^2 - 1} \\
&= \frac{4(-1)^{k+1}}{\pi(4k^2 - 1)}.
\end{aligned}$$

Importantly, since $|\cos(x)|$ is even and $\sin(nx)$ is odd, their product is also odd and thus integrates to zero over a symmetric interval (which results by taking the same approach as for a_k , i.e., the splitting into I_1 and I_2), implying that the b_k terms vanish. Thus, the following

calculation of a_0 completes the proof.

$$\begin{aligned}
a_0 &= \frac{1}{\pi} \int_0^{2\pi} |\cos(x)| dx \\
&= \frac{2}{\pi} \left(\int_0^{\frac{\pi}{2}} \cos(x) dx - \int_{\frac{\pi}{2}}^{\pi} \cos(x) dx \right) \\
&= \frac{2}{\pi} \left(\sin(x) \Big|_0^{\frac{\pi}{2}} - \sin(x) \Big|_{\frac{\pi}{2}}^{\pi} \right) \\
&= \frac{4}{\pi}.
\end{aligned}$$

□

Lemma 23. *The Fourier series of $f(x) := |\cos(x)|$ uniformly converges towards $(\mathcal{F}f)(x)$ for all $x \in \mathbb{R}$.*

Proof. This is a simple application of Dirichlet's Theorem [105] stating that Fourier series $(\mathcal{F}f)(x)$ of absolutely integrable 2π -periodic functions that have a finite number of local extrema as well as a finite number of finite discontinuities in each period $f(x)$ converge to $1/2 (\lim_{x \rightarrow a^+} f(x) + \lim_{x \rightarrow a^-} f(x))$. □

Corollary 7. *Let $T_n(\cos(x)) := \cos(nx)$ be defined as the Chebyshev polynomial of the first kind, then the substitution of $x \mapsto \arccos x$ into Lem. 23 yields*

$$|x| = f_\infty(x) := \frac{2}{\pi} + \frac{4}{\pi} \sum_{k=1}^{\infty} \frac{(-1)^{k+1}}{4k^2 - 1} T_{2k}(x), \quad (\text{C3})$$

as $T_n(x) = \cos(n \arccos x)$ for $x \in [-1, 1]$.

Lemma 24. *The following degree- d polynomial is an ε -approximation of $|x|$ for $x \in [-1, 1]$ and $\varepsilon = \mathcal{O}(1/d)$*

$$f_d(x) := \frac{2}{\pi} + \frac{4}{\pi} \sum_{k=1}^d \frac{(-1)^{k+1}}{4k^2 - 1} T_{2k}(x). \quad (\text{C4})$$

Proof. Let $\varepsilon > 0$. Based on Cor. 7, the truncation error $E_d(x) := ||x| - f_d(x)|$ can be computed via

$$\begin{aligned}
E_d(x) &= ||x| - f_d(x)| = |(\mathcal{F}f)(x) - f_d(x)| \\
&= \left| \frac{4}{\pi} \sum_{k=d+1}^{\infty} \frac{(-1)^{k+1}}{4k^2 - 1} T_{2k}(x) \right|.
\end{aligned}$$

Aiming to bound $E_d(x) \leq \varepsilon$, we acknowledge the bound $|T_{2k}(x)| \leq 1$ for $x \in [-1, 1]$, such that

$$\begin{aligned}
E_d(x) &\leq \frac{4}{\pi} \sum_{k=d+1}^{\infty} \left| \frac{(-1)^{k+1}}{4k^2 - 1} \right| \leq \frac{4}{\pi} \sum_{k=N+1}^{\infty} \frac{1}{4k^2 - 1} \\
&= \frac{4}{\pi} \sum_{k=d+1}^{\infty} \frac{1}{k^2} \frac{1}{4 - 1/k^2} \leq \frac{4}{3\pi} \sum_{k=d+1}^{\infty} \frac{1}{k^2} \\
&\leq \frac{4}{3\pi} \int_d^{\infty} \frac{1}{x^2} dx = \frac{4}{3\pi d} \leq \varepsilon
\end{aligned}$$

To satisfy $E_d(x) \leq \varepsilon$, we hence need $d \geq 4/3\pi\varepsilon$. □